SSRG International Journal of Electrical and Electronics Engineering
ISSN: 2348-8379/ https://doi.org/10.14445/23488379/IJEEE-V13I2P102

Volume 13 Issue 2, 15-37, February 2026

Original Article

A Proposed Adaptive Droop Controller for Hybrid Alternating Current / Direct Current Smart Microgrids

Om mohamed M. Elfadawy[1,*], Bishoy E. Sedhom[1], Ebrahim A. Badran[1,2], Ibrahim I. I. Mansy[1]

[1]*Electrical Engineering Department, Faculty of Engineering, Mansoura University, Mansoura, Egypt.*
[2]*Mansoura High Institute of Engineering and Technology, Ministry of Higher Education, Mansoura, Egypt.*

[*]*Corresponding Author : tota_tota81@yahoo.com*

Received: 11 November 2025 Revised: 16 December 2025 Accepted: 12 January 2026 Published: 17 February 2026

Abstract *- Smart hybrid microgrid power architectures encounter a critical challenge in achieving rapid power sharing while maintaining stable operation. This study introduces a novel adaptive droop-based control strategy designed to address this issue in smart hybrid microgrids under various operating conditions, including steady-state operation and load variations resulting from both load increases and decreases. Conventional droop control techniques employed in inverter-based smart hybrid microgrids are generally insufficient to ensure satisfactory performance, as increasing the droop gain to accelerate power sharing can adversely affect system stability. The proposed approach enhances primary control performance by optimally adjusting droop coefficients alongside voltage and/or current control loops. Consequently, it improves power quality indicators—such as frequency and voltage regulation—while preserving accurate active and reactive power sharing among interconnected smart hybrid microgrids. The developed control strategy effectively mitigates voltage and frequency deviations due to load sharing between inverters and then enhances overall power distribution performance. Simulation analyses conducted under diverse operating scenarios, including steady-state conditions and dynamic load changes, validate the proposed method. This demonstrates that the proposed controller significantly improves the overall stability of smart hybrid microgrids by increasing faster power sharing and reducing voltage and frequency fluctuations.*

Keywords *- Hybrid AC/DC Smart Microgrid, Droop controller, State-space, Voltage & Current controllers, Adaptive controller.*

1. Introduction

Smart Hybrid Microgrid (H-SMG) operation is characteristically classified into two distinct modes: Islanded Operating Mode (IOM) or Grid-Connected Mode (GCM). [1] A major task in the IOM procedure is confirming voltage/ frequency regulation and system stability. Attaining optimum power sharing among efficient load management, Distributed Generators (DGs), and seamless transitions amongst operative modes are critical for preserving the whole stability and performance of the SMG organism. [2] H-SMG operation demands power sharing amongst DGs in SMGs, and besides changing power amongst Alternating Current Smart Microgrid (AC-SMG) / Direct Current Smart Microgrid (DC-SMG). [3, 4] This paper introduces a novel adaptive droop control strategy designed to address the challenges encountered in H-SMGs in different cases: steady state conditions and changing the load value (reducing and increasing loads) to advance faster power sharing, and diminish fluctuations and variations in the voltage/frequency. Primary droop control is commonly employed to enable power sharing among distributed generators in both AC and/or DC smart microgrids [5, 6]. It operates through the innermost feedback and feedforward control loops at the converter level, regulating voltage and/or frequency in real time to ensure local system stability and effective load distribution. The secondary control layer is responsible for compensating steady-state deviations, such as voltage or frequency offsets introduced by the droop mechanism, by adjusting the reference values of the primary controller via a communication infrastructure [7]. In AC smart microgrids, real and reactive power sharing is typically achieved using droop control strategies based on the Power–Frequency and Reactive Power–Voltage magnitude relationships (P–F/Q–V). In contrast, DC smart microgrids commonly employ Voltage–Current (V–I) droop control to regulate power distribution. For hybrid smart microgrid configurations, several droop-based control schemes have been developed to ensure coordinated power exchange between AC and/or DC subsystems [8, 9]. Additionally, centralized control architectures have been adopted in hybrid AC/DC smart microgrids to manage overall power flow and system coordination [10]. However, this approach requires a rapid communication link to preserve the system stability and reliability. So as to develop this subject, a decentralized control scheme based on the droop scheme is suggested to share power among AC/ DC–SMG. A bidirectional droop is implemented for ILC by utilizing communal per unit (p.u.)

ranges of DC voltage or AC frequency. [11-13] Most existing studies on hybrid smart microgrids primarily focus on controlling the interlinking converter to enable power exchange between AC/DC smart grids, while largely sharing reactive power in AC grids and current sharing challenges in DC grids. Also, many reported interlinking converter control strategies rely on normalized Frequency/Voltage (F/V) droop control. In these approaches, p.u. of DC voltage and AC frequency are monitored. However, such control schemes introduce steady-state deviations in voltage and frequency [14, 15]. Then, supplementary control layers are commonly incorporated in AC and/or DC smart microgrid architectures. Once these variables are fully restored, power exchange between AC and DC smart microgrids diminishes to zero due to the absence of voltage or frequency deviations. These supplementary controllers are mainly intended to enhance the performance of the primary control layer, including voltage, current, and droop control loops. It is able to progress power qualities of the H-SMGs, for example, frequency or DC voltage, even while retaining appropriate power sharing between two SMGs. [16-18] NOVELTY, to solve the above problems, in this paper, a proposed adaptive droop control is recommended for active/ reactive power sharing, and voltage/ frequency restoration for H-SMG. A comparison between the primary and proposed controllers is discussed in different cases. The voltage/ frequency, current, and active/reactive powers are discussed.

It can be seen that the proposed control advances the system's stability margins, certifies faster power sharing, and diminishes fluctuations and variations in voltage/ frequency.

2. Literature Review

Several studies have addressed control strategies for hybrid microgrid systems. In [19], a hybrid control scheme was developed to enhance power quality in microgrids, particularly improving voltage performance under unbalanced and nonlinear load conditions. An adaptive droop control for the low-voltage AC/DC microgrids was presented in [20] to ensure accurate power transfer between sub-grids. In [21], a decentralized control approach based on V–I droop was proposed to improve the response of hybrid AC/DC microgrids and to achieve power sharing among AC and DC distributed energy resources. A centralized control framework for an autonomous hybrid microgrid comprising photovoltaic systems, wind turbines, battery storage, and a diesel generator was introduced in [22]. Furthermore, [23] investigated voltage stability in islanded microgrids using droop control techniques. Table 1 provides a comparative assessment between the proposed work and existing studies across several key performance criteria, including voltage and frequency restoration as well as active and reactive power sharing. The comparison indicates that the proposed approach successfully satisfies all evaluation criteria, whereas previous studies address only a subset of these objectives.

Table 1. A comparison between the literature review and the presented work

Ref	MG Type	Method	Voltage Restoration	Frequency Restoration	Active Power Sharing	Reactive Power Sharing
[1]	AC/DC- MG	adaptive droop control	√	√	×	×
[2]	DC -MG	Modified droop control	√	×	×	×
[24]	DC- MG	Improved droop control	√	×	×	×
[25]	DC-MG	Modified droop control	√	×	×	×
[26]	Hybrid AC/DC-MG	Modified adaptive droop control	×	×	√	√
[27]	H/ AC/DC- MG	Modified droop control	×	×	√	√
[28]	AC-MG	Modified droop control	√	×	×	×
[29]	H/ AC/DC- MG	Modified droop control	√	×	×	×
[30]	H/ AC/DC- MG	Modified droop control	×	√	√	√
[31]	- AC- MG -H/ AC/DC- MG	Modified droop control	√	√	×	×
[32]	AC - MG	Modified droop control	√	×	√	√
This research	H/ AC/DC- MG	Proposed droop control	√	√	√	√

The essential contributions of this paper can be summarized as surveys.

1. Offering a suggested adaptive droop controller for the SMG to develop the primary controller's performance for H-SMG.
2. Offering a proportional analysis between the recommended controller and the conventional droop control at steady state.
3. Offering a proportional analysis among the proposed control and the conventional droop control in exchanging the loads of SMG.

This work is organized as follows. Section 2 appraises the architecture of SMG's system. Sections 3, 4, 5, and 6 represent the AC–SMG, DC–SMG, ILC, and SMG complete state space modeling, respectively. Section 7 displays the primary droop control, and Section 8 presents the simulation results. Finally, Section 9 concludes the paper.

3. The Proposed System Architecture

A Hybrid Smart Microgrid (H-SMG) is formed through the integrated operation of AC and DC generation units and loads. The DC smart microgrid consists of DC energy sources-such as photovoltaic systems and permanent magnet synchronous generator–based wind turbines—along with battery energy storage systems, DC loads, and associated power electronic interfaces, including DC–DC boost converters, thereby constituting the DC sub-grid. Conversely, the AC smart microgrid comprises AC loads that are interconnected with the DC side via a voltage source converter. The AC and/or DC sub-grids are coupled through an H-SMG architecture. These interlinking converters play a vital role in enhancing system reliability and facilitating power exchange between the sub-grids, as illustrated in Figure 1.

4. State Space Modeling of AC - SMG

The distributed energy resources are assumed to be ideal voltage source converters, and a droop-based primary control strategy is adopted to enable power sharing among them [33]. The dynamic behavior of the power output of the nth DER is derived using Park transformation, Taylor series–based linearization, and fundamental circuit laws, while accounting for the associated RLC filter components [34].

4.1. DER Power

$$\Delta \dot{i}_{d}^{n} = -\left(\Re_{fn}/\mathrm{L}_{fn}\right)\Delta i_{d}^{n} + \omega\Delta i_{q}^{n} - \left(1/\mathrm{L}_{fn}\right)\Delta \mathcal{V}_{od}^{n} + \left(1/\mathrm{L}_{fn}\right)\Delta \mathcal{E}_{d}^{n} - i_{qo}^{n}\,\Delta\omega_{n} \tag{1}$$

$$\Delta \dot{i}_{q}^{n} = -\omega\Delta i_{d}^{n} - \left(\Re_{fn}/\mathrm{L}_{fn}\right)\Delta i_{q}^{n} - \left(1/\mathrm{L}_{fn}\right)\Delta \mathcal{V}_{oq}^{n} + \left(1/\mathrm{L}_{fn}\right)\Delta \mathcal{E}_{q}^{n} - i_{do}^{n}\,\Delta\omega_{n} \tag{2}$$

$$\Delta \dot{\mathcal{V}}_{od}^{n} = -\left(1/\mathrm{C}_{fn}\right) i_{d}^{n} + \omega\Delta \mathcal{V}_{oq}^{n} - \left(1/\mathrm{C}_{fn}\right)\Delta i_{od}^{n} + \mathcal{V}_{oqo}^{n}\Delta\omega_{n} \tag{3}$$

$$\Delta \dot{\mathcal{V}}_{oq}^{n} = \left(1/\mathrm{C}_{fn}\right) i_{q}^{n} - \omega\Delta \mathcal{V}_{oq}^{n} - \left(1/\mathrm{C}_{fn}\right)\Delta i_{oq}^{n} - \mathcal{V}_{odo}^{n}\Delta\omega_{n} \tag{4}$$

Where $\mathcal{E}_{d}^{n}$ and$\mathcal{E}_{q}^{n}$ are the $dq -$ components of $\mathcal{E}^{n}$, 0.

A DER state space demonstration can be identified

As:

$$\dot{\mathrm{X}}_{p}^{n} = \mathrm{A}_{p}^{n}\,\mathrm{X}_{p}^{n} + \mathcal{B}_{p}^{n}\,\mathrm{U}_{p}^{n} + \mathcal{B}_{p\mathcal{N}}^{n}\,\mathrm{U}_{\mathcal{PN}}^{n} \tag{5}$$

$$\dot{\mathcal{Y}}_{p}^{n} = \mathcal{C}_{p}^{n}\,\mathrm{X}_{p}^{n} + \mathcal{D}_{p}^{n}\,\mathrm{U}_{p}^{n} + \mathcal{D}_{\mathcal{PN}}^{n}\,\mathrm{U}_{\mathcal{PN}}^{n} \tag{6}$$

Where

$\mathrm{X}_{p}^{n} = \left|i_{dq}^{n} \quad \Delta\mathcal{V}_{odq}^{n}\right|^{\mathcal{T}}$, $\mathrm{U}_{p}^{n} = \left|\Delta\mathcal{E}_{dq}^{n} \quad \Delta\omega_{n}\right|^{\mathcal{T}}$ is th control input, and the

disturbance inputs are $\mathrm{U}_{\mathcal{PN}}^{n} = \Delta i_{dq}^{n}$, $\mathcal{B}_{p}^{n} = \left|0_{2} \quad -\left(1/\mathrm{C}_{fn}\right)\mathrm{I}_{2}\right|^{\mathcal{T}}$, $\mathrm{C}_{p}^{n} = \mathrm{I}_{4}$, $\mathcal{D}_{p}^{n} = 0$, $\mathcal{D}_{\mathcal{PN}}^{n} = 0$

$$A_{p}^{n} = \begin{vmatrix} -\Re_{f}^{n}/L_{f}^{n} & \omega & -1/L_{f}^{n} & 0 \\ -\omega & -\Re_{f}^{n}/L_{f}^{n} & 0 & -1/L_{f}^{n} \\ 1/C_{f}^{n} & 0 & 0 & \omega \\ 0 & 1/C_{f}^{n} & -\omega & 0 \end{vmatrix}$$

$$\mathcal{B}_{p}^{n} = \begin{vmatrix} 1/L_{f}^{n} & 0 & -i_{qo}^{n} \\ 0 & 1/L_{f}^{n} & -i_{do}^{n} \\ 0 & 0 & -\mathcal{V}_{od}^{n} \end{vmatrix}$$

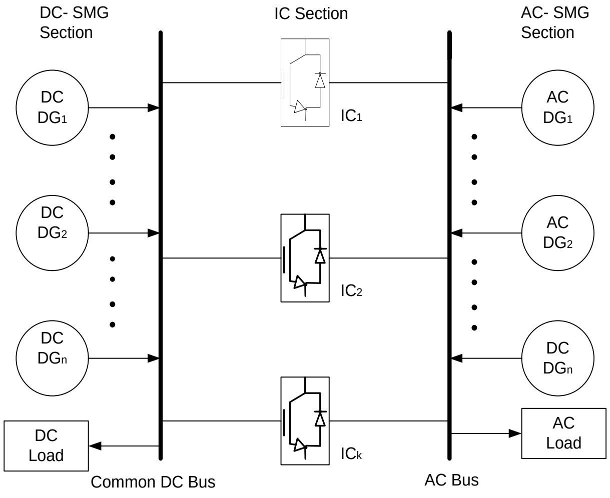

Fig. 1 Islanded H-SMG architecture

4.2. Power Network

The comprising DERs linking lines are supposed to be presented [35]. The power network dynamic model (n) line is:

$$\Delta \dot{i}_{od}^{n} = \left(\Re_{i}^{n}/\mathrm{L}_{i}^{n}\right)\Delta i_{od}^{n} + \omega\Delta i_{oq}^{n} - \left(1/\mathrm{L}_{i}^{n}\right)\Delta \mathcal{V}_{od}^{n} - \left(1/\mathrm{L}_{i}^{n}\right)\Delta \mathcal{V}_{pcc\cdot d}^{n} + i_{qo}^{n}\,\Delta\omega_{c}^{n} \tag{7}$$

$$\Delta \dot{i}_{oq}^{n} = -\omega\Delta i_{od}^{n} - \left(\Re_{i}^{n}/\mathrm{L}_{i}^{n}\right)\Delta i_{oq}^{n} + \left(1/\mathrm{L}_{i}^{n}\right)\Delta \mathcal{V}_{oq}^{n} - \left(1/\mathrm{L}_{i}^{n}\right)\Delta \mathcal{V}_{pcc\cdot q}^{n} - \mathrm{i}_{od0}^{n}\,\Delta\omega_{c}^{n} \tag{8}$$

Where$\Delta\omega_{\mathfrak{c}}^{n}$ is the perturbed frequency.
A power network state space procedure is: -

$$\dot{X}_{\mathrm{ps}}^{n} = A_{\mathrm{ps}}^{n} X_{\mathrm{ps}}^{n} + B_{\mathfrak{s}\mathcal{H}}^{n} U_{\mathfrak{s}\mathcal{H}}^{n} + B_{\mathrm{sp}}^{n} U_{\mathrm{sp}}^{n} + B_{\mathrm{s}\mathcal{g}}^{n} U_{\mathrm{s}\mathcal{g}}^{n} \quad (9)$$

$$\dot{Y}_{\mathrm{ps}}^{n} = \mathcal{C}_{\mathrm{ps}}^{n} X_{\mathrm{ps}}^{n} \quad (10)$$

Where

$$X_{\mathrm{ps}}^{n} = Y_{\mathrm{ps}}^{n} = \mathfrak{i}_{\mathrm{o}dq}^{n}, U_{\mathrm{sp}}^{n} = \Delta\mathcal{V}_{\mathfrak{p}cc\cdot dq}^{n}, U_{\mathfrak{s}\mathcal{K}}^{n} = Y_{\mathcal{K}\mathfrak{s}}^{n}, U_{\mathrm{s}\mathcal{g}}^{n} = \Delta\omega_{\mathfrak{c}}^{\mathrm{n}} \quad (11)$$

4.3. *Load of AC-SMG*

The series RL is supposed to be for every SMG, respectively, and the no. of AC-MG loads is (m).

The RL load state space model may be characterized as presented:

$$\dot{X}_{\mathcal{KJ}}^{m} = A_{\mathcal{KJ}}^{m} X_{\mathcal{KJ}}^{m} + B_{\mathcal{KJ}c}^{m} U_{\mathcal{KJ}c}^{m} + B_{\mathcal{KJ}\mathfrak{p}}^{m} U_{\mathcal{KJ}\mathfrak{p}}^{m} \quad (12)$$

$$\dot{\mathcal{Y}}_{\mathcal{KJ}}^{m} = \mathcal{C}_{\mathcal{KJ}}^{m} X_{\mathcal{KJ}}^{m} \quad (13)$$

Where

$$Y_{\mathcal{KJ}}^{m} = \Delta\mathfrak{i}_{\circ dq}^{m} = X_{\mathcal{KJ}}^{m}$$

and $Y_{\mathcal{KJ}c}^{m} = \Delta\omega_{\mathfrak{c}}^{m}, U_{\mathcal{KJ}\mathfrak{p}}^{m} = \Delta\mathcal{V}_{\mathfrak{p}cc\cdot dq}^{m}$

4.4. *Power Controller*

The power control of every DER comprises a power calculator, two LPFs, ω-P, $\mathcal{V}_d - \mathcal{Q}d$roop characteristics, and voltage phase is σ_n .

$$\Upsilon_n = \sigma_n - \sigma_{\mathfrak{c}}^{m} = \int(\omega_n - \omega_{\mathfrak{c}}^{m})\mathrm{d}t \quad (14)$$

$$\Upsilon_n = \omega - \omega_{\mathfrak{c}} \quad (15)$$

Wherever the frequency of DERn is ω_m , and $\omega_{\mathfrak{c}}^{m}$ is the DER1voltage phase.

$$\dot{X}_{\mathcal{PCO}}^{n} = A_{\mathcal{PCO}}^{n} X_{\mathcal{PCO}}^{n} + B_{\mathcal{PCO}}^{n} U_{\mathcal{PCO}}^{n} + B_{\mathrm{C}}^{n} \Delta\omega_{\mathfrak{c}}^{m} \quad (16)$$

$$\dot{Y}_{\mathcal{PCO}}^{n} = \mathcal{C}_{\mathcal{PCO}}^{n} \mathcal{X}_{\mathcal{PCO}}^{n} \quad (17)$$

Where:-

$$X_{\mathfrak{p}c\mathrm{D}}^{m} = |\Delta\Upsilon_n \quad \Delta\mathcal{P}_n \quad \Delta\mathcal{Q}_n|^{\mathcal{T}},\ U_{\mathfrak{p}c\mathrm{D}}^{n} = |Y_{\mathrm{D}\mathfrak{po}}^{n} \quad Y_{\mathfrak{po}\mathrm{I}}^{n}|^{\mathcal{T}}, Y_{\mathfrak{p}c\mathrm{D}}^{m} = \left|\Delta\omega_n \quad \Delta\mathcal{V}_{d\mathrm{q.r}}^{n} \quad \Delta\Upsilon_n\right|^{\mathcal{T}},\ B_{\mathfrak{p}c\mathrm{D}}^{n} = |B_{\mathfrak{po}\mathrm{D}\mathfrak{p}}^{n} \quad B_{\mathfrak{pop}\mathrm{I}}^{n}|^{\mathcal{T}}$$

$$A_{\mathrm{po}}^{n} = \begin{vmatrix} 0 & -\omega_{\mathfrak{c}} & 0 \\ 0 & 0 & -\omega_{\mathfrak{c}} \end{vmatrix}$$

$$B\mathfrak{p}_{\mathfrak{p}c}^{n} = \begin{vmatrix} 0 & 0 \\ \omega_{\mathfrak{c}}\mathcal{V}_{\mathfrak{o}do}^{n} & \omega_{\mathfrak{c}}\mathcal{V}_{\mathfrak{o}qo}^{n} \\ -\omega_{\mathfrak{c}}\mathcal{V}_{\mathfrak{o}qo}^{n} & \omega_{\mathfrak{c}}\mathcal{V}_{\mathfrak{o}do}^{n} \end{vmatrix}$$

$$B\mathfrak{p}_{\mathfrak{p}}^{n} = \begin{vmatrix} 0 & 0 & 0 & 0 \\ 0 & 0 & \omega_{\mathfrak{c}}\mathcal{V}_{\mathfrak{o}do}^{n} & \omega_{\mathfrak{c}}\mathcal{V}_{\mathfrak{o}qo}^{n} \\ 0 & 0 & \omega_{\mathfrak{c}}\mathcal{V}_{\mathfrak{o}qo}^{n} & -\omega_{\mathfrak{c}}\mathcal{V}_{\mathfrak{o}do}^{n} \end{vmatrix}$$

$$\mathcal{C}_{\mathrm{po}}^{n} = \begin{vmatrix} 0 & -\mathfrak{m}_{\mathfrak{p}}^{n} & 0 \\ 0 & 0 & -n_{q}^{n} \\ 1 & 0 & 0 \end{vmatrix}$$

$$B_{c}^{n} = \begin{vmatrix} 0 \\ 1 \end{vmatrix}$$

4.5. *Voltage Controller*

Each distributed energy resource operating in islanded mode is equipped with a voltage control loop to regulate its terminal voltage. The reference value of the direct-axis component is derived from the droop control characteristic, while the quadrature-axis reference is maintained at zero.

A voltage controller state space representation may be known as:

$$\dot{X}_{\mathcal{V}}^{n} = A_{\mathcal{V}}^{\mathfrak{n}} X_{\mathcal{V}}^{\mathfrak{n}} + B_{\mathcal{V}}^{n} U_{\mathcal{V}}^{n} + B_{\mathcal{V}}^{\mathfrak{n}} U_{\mathcal{V}}^{\mathfrak{n}} \quad (18)$$

$$\mathcal{Y}Y_{\mathcal{V}}^{n} = \mathcal{C}_{\mathcal{V}}^{n} X_{\mathcal{V}}^{n} + D_{\mathcal{V}}^{n} U_{\mathcal{V}}^{n} \quad (19)$$

Where,

$$D_{\mathcal{V}}^{n} = |D_{\mathcal{V}\mathrm{D}\mathfrak{p}}^{n} \quad D_{\mathcal{V}\mathfrak{p}}^{n}|, Y_{\mathcal{V}}^{\mathfrak{m}} = \Delta\mathfrak{i}_{d\mathrm{q.r}}^{n},\ U_{\mathcal{V}}^{n} = |Y_{\mathrm{D}\mathfrak{p}a}^{n} \quad Y_{\mathfrak{pa}\mathrm{I}}^{n}|^{\mathcal{T}}, A_{\mathfrak{c}}^{n} = 0,\ \mathcal{C}_{\mathfrak{c}}^{\mathfrak{n}} = I_2, \mathcal{B}_{\mathcal{V}}^{n} = |B_{\mathcal{V}\mathrm{D}\mathfrak{p}}^{n} \quad B_{\mathcal{V}\mathfrak{p}}^{n}|$$

$$D_{\mathcal{V}\mathfrak{p}}^{\mathfrak{n}} = \begin{vmatrix} -\mathcal{C}^{m}\mathcal{V}_{\mathfrak{o}qo}^{n} & K_{\mathfrak{p}\mathcal{V}} & 0 \\ \mathcal{C}^{m}\mathcal{V}_{\mathfrak{o}do}^{n} & 0 & K_{\mathfrak{p}\mathcal{V}} \end{vmatrix}$$

4.6. *Current Controller*

The voltage across the filter inductor must be designed by the current controller to lessen the current error, certifying a quick dynamic response while preserving system stability. The PI controller is commonly implemented because of its capability to alter both proportional and integral gains, which helps to accomplish a stable compromise between changing load and steady-state performance. Proper tuning of the PI control is important to realize an ideal balance between fast response and robustness against disturbances [36].

The current controller state space model is:

$$\dot{X}_{c}^{n} = A_{c}^{n} X_{c}^{n} + B_{c}^{\mathfrak{n}} U_{c}^{n} + B_{c}^{\mathfrak{n}} U_{c}^{n} \quad (20)$$

$$Y_{c}^{n} = \mathcal{C}_{c}^{n} X_{c}^{n} + D_{c}^{n} U_{c}^{n} \quad (21)$$

Where,

$$\mathrm{U}_{\mathrm{c}}^{n} = |\mathrm{Y}_{\mathrm{Dp}}^{n} \quad \mathrm{Y}_{\mathrm{c}}^{n} \quad \Delta\omega_{n}|^{\mathcal{T}}, \mathrm{Y}_{\mathcal{V}}^{n} = m_{dq}^{n}, \mathcal{D}_{\mathcal{V}}^{n} = |\mathcal{D}_{c\mathrm{Dp}}^{n} \quad \mathcal{D}_{c\mathcal{V}}^{n} \quad \mathcal{D}_{c\mathrm{p}}^{n}|, \mathrm{A}_{\mathrm{c}}^{n} = 0, \mathcal{C}_{\mathrm{c}}^{n} = \mathrm{I}_2, \mathcal{B}_{\mathcal{V}}^{n} = |\mathcal{B}_{c\mathrm{Dp}}^{n} \quad \mathcal{B}_{c\mathcal{V}}^{n} \quad \mathcal{B}_{c\mathrm{p}}^{n}|$$

$$\mathrm{D}_{c\mathrm{p}}^{n} = \begin{vmatrix} -\mathrm{K}_{\mathrm{pi}} & -\omega_{no}\mathrm{L}^{n} & 1 & 0 \\ \omega_{no}\mathrm{L}^{n} & -\mathrm{K}_{\mathrm{pi}} & 0 & 1 \end{vmatrix}$$

4.7. Common Reference Frame

The variables in the CRF and individual frames are $\mathcal{V}_{DQ}$ *and* $\mathcal{V}_{dq}$ correspondingly,

$$\Delta\mathcal{V}_{DQ} = \mathcal{T}_{s}\Delta\mathcal{V}_{dq}^{n} + \mathcal{T}_{\gamma 1}\Delta\gamma \tag{22}$$

$$\Delta\mathcal{V}_{dq} = \mathcal{T}_{s}^{-1}\Delta\mathcal{V}_{DQ}^{\mathrm{n}} + \mathcal{T}_{\gamma 2}\Delta\gamma \tag{23}$$

$$\mathcal{T}_{s} = \begin{vmatrix} \cos\gamma_0 & -\sin\gamma_0 \\ \sin\gamma_0 & \cos\gamma_0 \end{vmatrix} \tag{24}$$

$$\mathcal{T}_{\gamma 1} = \begin{vmatrix} -\mathcal{V}_{0d}\sin\gamma_0 & -\mathcal{V}_{0q}\cos\gamma_0 \\ \mathcal{V}_{0d}\cos\gamma_0 & -\mathcal{V}_{0q}\sin\gamma_0 \end{vmatrix} \tag{25}$$

$$\mathcal{T}_{\gamma 2} = \begin{vmatrix} -\mathcal{V}_{0d}\sin\gamma_0 & +\mathcal{V}_{0q}\cos\gamma_0 \\ -\mathcal{V}_{0d}\cos\gamma_0 & -\mathcal{V}_{0q}\sin\gamma_0 \end{vmatrix} \tag{26}$$

4.8. Complete AC-SMG State Space Modeling

The DQ frame rotating frequency is = ω_{n}

$$\Delta\,\omega_{\mathrm{c}} = \mathrm{D}_{\omega}\ \omega \tag{27}$$

Wherever D_{ω} is the dimension M reference incidence vector.

$$\gamma_{n} = \int(\omega_{n} - \omega_{\mathrm{c}}^{m})\mathrm{d}t \tag{28}$$

$$\Delta\dot{\gamma} = \left(\mathrm{A}_{\gamma_{\omega,1}} - \mathrm{A}_{\gamma_{\omega,2}}\mathrm{D}_{\omega}\right)\Delta\omega \tag{29}$$

$$\Delta\gamma = |\Delta\gamma_1 \quad \Delta\gamma_2 \quad \cdots \Delta\gamma_{\mathrm{M}}|^{\mathcal{T}} \tag{30}$$

$$\Delta\mathcal{V}_{\mathrm{bus,DQ}} = \mathcal{C}_{\mathrm{t}}^{\mathrm{ac}}\Delta\mathcal{V}_{\mathrm{inv},dq} + \mathcal{C}_{\mathcal{V}_{\mathrm{bus}}^{\mathrm{ac}}\gamma}\Delta\gamma \tag{31}$$

Where,

$$\mathcal{C}_{\mathrm{t}}^{\mathrm{ac}} = \begin{vmatrix} \cos\gamma_0 \\ \sin\gamma_0 \end{vmatrix}$$

$$\mathcal{C}_{\mathcal{V}_{\mathrm{bus}}^{\mathrm{ac}}\gamma} = \begin{vmatrix} -\mathcal{V}_{0d}\sin\gamma_0 \\ \mathcal{V}_{0d}\cos\gamma_0 \end{vmatrix}$$

$$\Delta\mathcal{V}_{\mathrm{DQ}} = \mathcal{C}_{\mathrm{t}}^{\mathrm{ac}}\Delta\mathcal{V}_{\mathrm{inv},dq} + \mathcal{C}_{\mathcal{V}_{\mathrm{bus}}^{\mathrm{ac}}\gamma}\Delta\gamma \tag{32}$$

$$\Delta\mathrm{I}_{DQ} = \mathcal{C}_{\mathcal{T}}^{\mathrm{ac}}\Delta\mathrm{I}_{\mathrm{in},dq} + \mathcal{C}_{\mathrm{I}_{\mathrm{in,DD}}\gamma}\Delta\gamma \tag{33}$$

Where,

$$\mathcal{C}_{\mathcal{T}}^{\mathrm{ac}} = \begin{vmatrix} \cos\gamma_0 & -\sin\gamma_0 \\ \sin\gamma_0 & \cos\gamma_0 \end{vmatrix}$$

$$\mathcal{C}_{\mathfrak{I}_{\mathrm{in},\mathfrak{DQ}}\gamma} = \begin{vmatrix} -\mathrm{I}_{0d}\sin\gamma_0 & +\mathrm{I}_{0q}\cos\gamma_0 \\ -\mathrm{I}_{0d}\cos\gamma_0 & -\mathrm{I}_{0q}\sin\gamma_0 \end{vmatrix}$$

$$\Delta\mathcal{V}_{\mathrm{l}}^{ac} = \mathcal{D}_{\mathrm{l,bus}}^{ac}\,\Delta\mathcal{V}_{bus}^{ac} \tag{34}$$

Where,,

$$\left(\mathcal{D}_{\mathrm{l,bus}}^{ac}\right)^{\mathcal{T}}\Delta\mathrm{I}_{\mathrm{l}}^{ac} + \Delta\mathrm{I}_{\mathrm{lo}}^{ac} - \Delta\mathrm{I}_{\mathrm{out}}^{ac} = \Delta\mathrm{I}_{iv,DQ}$$

$$\Delta\mathrm{I}_{\mathrm{out}}^{ac} = \left|\Delta\mathrm{I}_{\mathrm{out},1}^{ac,\mathrm{D}}\ \Delta\mathrm{I}_{\mathrm{out},1}^{ac,Q} \quad \Delta\mathrm{I}_{\mathrm{out},2}^{ac,\mathrm{D}} \quad \Delta\mathrm{I}_{\mathrm{out},2}^{ac,Q} \cdots \Delta\mathrm{I}_{\mathrm{out,M}}^{ac,\mathrm{D}}\ \Delta\mathrm{I}_{\mathrm{out,M}}^{ac,Q}\right|^{\mathcal{T}}$$

AC section state space modeling is:

$$\dot{\mathrm{X}}_{AC} = \mathrm{A}_{AC}\,\mathrm{X}_{AC} + \mathrm{B}_{AC}\,\Delta\mathrm{I}_{\mathrm{out}}^{\mathrm{ac}} \tag{35}$$

$$\mathrm{X}_{AC} = \begin{bmatrix} \Delta\gamma \\ \Delta\omega \\ \Delta\mathcal{V}_{iv} \\ \Delta\mathrm{I}_{\mathrm{l}}^{\mathrm{ac}} \\ \Delta\mathrm{I}_{\mathrm{lo}}^{\mathrm{ac}} \end{bmatrix}$$

$$\mathrm{B}_{AC} = \begin{bmatrix} 0 \\ \mathrm{B}_{\omega\mathrm{I}_{\mathrm{in},dq}}(\mathcal{C}_{\mathcal{T}}^{\mathrm{ac}})^{-1} \\ \mathrm{B}_{\mathcal{V}_{\mathrm{in}}\mathrm{I}_{\mathrm{in},dq}}(\mathcal{C}_{\mathcal{T}}^{\mathrm{ac}})^{-1} \\ 0 \\ 0 \end{bmatrix}$$

$$\mathrm{A}_{AC} = \begin{bmatrix} 0 & \mathrm{A}_{\gamma_{\omega,1}} - \mathrm{A}_{\gamma_{\omega,2}}\mathcal{D}_{\omega} & 0 & 0 & 0 \\ -\mathrm{B}_{\omega\mathrm{I}_{\mathrm{in},dq}}(\mathcal{C}_{\mathcal{T}}^{\mathrm{ac}})^{-1}\left(\mathcal{C}_{\mathrm{I}_{iv,\mathrm{DQ}}\gamma}\right) & \mathrm{A}_{\omega} & \mathrm{A}_{\omega,\mathcal{V}_{\mathrm{inv}}} & \mathrm{B}_{\omega\mathrm{I}_{\mathrm{in},dq}}(\mathcal{C}_{\mathrm{t}}^{\mathrm{ac}})^{-1}\left(\mathcal{D}_{\mathrm{l,bus}}^{ac}\right)^{\mathcal{T}} & \mathrm{B}_{\omega\mathrm{I}_{\mathrm{in},dq}}(\mathcal{C}_{\mathrm{t}}^{\mathrm{ac}})^{-1} \\ -\mathrm{B}_{\mathcal{V}_{\mathrm{in}}\mathrm{I}_{\mathrm{in},dq}}(\mathcal{C}_{\mathcal{T}}^{\mathrm{ac}})^{-1}\left(\mathcal{C}_{\mathrm{I}_{iv,\mathrm{DQ}}\gamma}\right) & 0 & \mathrm{A}_{\mathcal{V}_{\mathrm{inv}}} & \mathrm{B}_{\mathcal{V}_{\mathrm{in}}\mathrm{I}_{\mathrm{in},dq}}(\mathcal{C}_{\mathrm{t}}^{\mathrm{ac}})^{-1}\left(\mathcal{D}_{\mathrm{l,bus}}^{ac}\right)^{\mathcal{T}} & \mathrm{B}_{\mathcal{V}_{\mathrm{in}}\mathrm{I}_{\mathrm{in},dq}}(\mathcal{C}_{\mathrm{t}}^{\mathrm{ac}})^{-1} \\ \mathrm{B}_{\mathrm{I}_{\mathrm{l}}^{ac}\mathcal{V}_{\mathrm{l}}^{ac}}\mathcal{D}_{\mathrm{l,bus}}^{ac}\,\mathcal{C}_{\mathcal{V}_{\mathrm{bus}}^{ac}\gamma} & \mathrm{B}_{\mathrm{I}_{\mathrm{l}}^{ac}\omega}\mathcal{D}_{\omega} & \mathrm{B}_{\mathrm{I}_{\mathrm{l}}^{ac}\mathcal{V}_{\mathrm{l}}^{ac}}\mathcal{D}_{\mathrm{l,bus}}^{ac}\,\mathcal{C}_{\mathrm{t}}^{ac} & \mathrm{A}_{\mathrm{I}_{\mathrm{l}}^{ac}} & 0 \\ \mathrm{B}_{\mathrm{I}_{\mathrm{lo}}^{ac}\mathcal{V}_{\mathrm{l}}^{ac}}\,\mathcal{C}_{\mathcal{V}_{\mathrm{bus}}^{ac}\gamma} & \mathrm{B}_{\mathrm{I}_{\mathrm{lo}}^{ac}\omega}\mathcal{D}_{\omega} & \mathrm{B}_{\mathrm{I}_{\mathrm{lo}}^{ac}\mathcal{V}_{\mathrm{lo}}^{ac}}\,\mathcal{C}_{\mathrm{t}}^{ac} & 0 & \mathrm{A}_{\mathrm{I}_{\mathrm{l}}^{ac}} \end{bmatrix}$$

5. DC-SMG State Space Modeling

5.1. DC- DER Power

DC- sector is demonstrated as:

$$\mathcal{V}_{\mathrm{con,DC}} = \mathcal{V}_{\mathrm{con,DC}}^{*} - \mathrm{H}_{\mathrm{P,DC}}\left(\mathrm{P}_{\mathrm{con,DC}}^{\mathrm{meas}} - \mathrm{P}_{\mathrm{con,DC}}^{*}\right) \tag{36}$$

$$P_{\mathfrak{con},DC}^{\mathfrak{meas}} = \frac{\omega_{\mathfrak{c}}}{\omega_{\mathfrak{c}}+f} P_{\mathfrak{con},DC}$$

Wherever interlinking converter = f, low pass filter cut − off frequency $\omega_{\mathfrak{c}}$.
DC/DC converter power output.

$$P_{\mathfrak{con},DC} = \mathcal{V}_{\mathfrak{con},DC}\ I_{\mathfrak{con},DC} \tag{37}$$

5.2. *DC-DC Converter State Space Model*

$$\Delta\mathcal{V}_{\mathfrak{con}}^{*} = A_{\mathcal{V}_{\mathfrak{Con}}}\Delta\mathcal{V}_{\mathfrak{con}} + B_{\mathcal{V}_{\mathfrak{con}}\,I_{\mathfrak{con}}}\Delta I_{\mathfrak{con}} \tag{38}$$

Where

$$\Delta\mathcal{V}_{\mathfrak{con}} = |\Delta\mathcal{V}_{\mathfrak{con},1} \quad \Delta\mathcal{V}_{\mathfrak{con},2} \quad \cdots \Delta\mathcal{V}_{\mathfrak{con},M}|^{\mathcal{T}}$$

$$\Delta\mathcal{J}_{\mathfrak{Con}} = |\Delta\mathcal{J}_{\mathfrak{con},1} \quad \Delta\mathcal{J}_{\mathfrak{con},2} \quad \cdots \Delta\mathcal{J}_{\mathfrak{con},\mathcal{M}}|^{\mathcal{T}}$$

$$A_{\mathcal{V}_{\mathfrak{Con}}} = \mathcal{d}\mathfrak{iag}\left\{\left[\left(-\omega_{\mathfrak{c}} \ -H_{P,1}\ \omega_{\mathfrak{c}}\ I_{\mathcal{V}_{\mathfrak{con},1}}^{(0)}\right) \ \left(-\omega_{\mathfrak{c}} \ -H_{P,2}\ \omega_{\mathfrak{c}}\ I_{\mathcal{V}_{\mathfrak{con},2}}^{(0)}\right) \cdot \cdot\cdot \left(-\omega_{\mathfrak{c}} \ -H_{P,\mathcal{M}}\ \omega_{\mathfrak{c}}\ I_{\mathcal{V}_{\mathfrak{con},M}}^{(0)}\right)\right.\right.$$

$$B_{\mathcal{V}_{\mathfrak{con}}} = \mathcal{d}\mathfrak{iag}\left\{\left[\ \left(-H_{P,2}\ \omega_{\mathfrak{c}}\ \mathcal{V}_{\mathcal{V}_{\mathfrak{con},2}}^{(0)}\right)\left(-H_{P,2}\ \omega_{\mathfrak{c}}\ \mathcal{V}_{\mathfrak{c_{on,2}}}^{(0)}\right) \cdot \cdot\cdot \left(-H_{P,\mathcal{M}}\ \omega_{\mathfrak{c}}\ \mathcal{V}_{\mathcal{V}_{\mathfrak{con},M}}^{(0)}\right)\right]\right\}$$

Wherever the number of DC section power lines = H

5.3. *DC Current Control*

$$X^{\cdot\mathfrak{n}}_{c,dc} = A^{\mathfrak{n}}_{c,dc}X^{\mathfrak{n}}_{c,dc} + B^{\mathfrak{n}}_{c,dc}\, U^{\mathfrak{n}}_{c,dc} \tag{39}$$

$$\mathcal{Y}^{\mathfrak{n}}_{c,dc} = \mathcal{C}^{\mathfrak{n}}_{c,dc}\, X^{\mathfrak{n}}_{c,dc} + \mathcal{D}^{\mathfrak{n}}_{c,dc}\, U^{\mathfrak{n}}_{c,dc} \tag{40}$$

Where,

$U^{\mathfrak{n}}_{\mathfrak{c},dc} = \left|Y^{\mathfrak{n}}_{D\mathfrak{p},dc} \quad Y^{\mathfrak{n}}_{\mathfrak{c},dc} \quad \Delta\omega_{\mathfrak{n},dc}\right|^{\mathcal{T}}$, $Y^{\mathfrak{n}}_{\mathcal{V},dc} = \mathcal{m}^{\mathfrak{n}}_{d\mathfrak{q},dc}$, $\mathcal{D}^{\mathfrak{n}}_{\mathcal{V},dc} = \left|\mathcal{D}^{\mathfrak{n}}_{cD\mathfrak{p},dc} \quad \mathcal{D}^{\mathfrak{n}}_{c\mathcal{V},dc} \quad \mathcal{D}^{\mathfrak{n}}_{c\mathfrak{p},dc}\right|$, $A^{\mathfrak{n}}_{\mathfrak{c},dc} = 0$, $\mathcal{C}^{\mathfrak{n}}_{\mathfrak{c},dc} = I_2$, $B^{\mathfrak{n}}_{\mathcal{V},dc} = \left|B^{\mathfrak{n}}_{cD\mathfrak{p},dc} \quad B^{\mathfrak{n}}_{c\mathcal{V},dc} \quad B^{\mathfrak{n}}_{c\mathfrak{p},dc}\right|$

$$\mathcal{D}^{\mathfrak{n}}_{c\mathfrak{p},dc} = \begin{vmatrix} -H_{\mathfrak{pi},dc} & -\omega_{\mathfrak{no},dc}\, L^{\mathfrak{n}}_{dc} & 1 & 0 \\ \omega_{\mathfrak{no},dc} L^{\mathfrak{n}}_{dc} & -H_{\mathfrak{pi},dc} & 0 & 1 \end{vmatrix}$$

5.4. *DC Power Line*

The DC sector is sculpted as a series resistor and indicator:

$$\mathcal{V}^{dc}_{\mathfrak{l},\mathfrak{R}} = L^{dc}_{\mathfrak{l},\mathfrak{R}}\frac{d}{dt}\, I^{dc}_{\mathfrak{l},\mathfrak{R}} + L^{dc}_{\mathfrak{l},\mathfrak{R}}\ I^{dc}_{\mathfrak{l},\mathfrak{R}} \tag{41}$$

5.5. *DC lines State Space Model*

$$\Delta I^{*dc}_{\mathfrak{l},\mathfrak{R}} = A_{I^{dc}_{\mathfrak{l}}}\Delta I^{dc}_{\mathfrak{l}} + B_{I^{dc}_{\mathfrak{l}}\mathcal{V}^{dc}_{\mathfrak{l}}}\Delta\mathcal{V}^{dc}_{\mathfrak{l}} \tag{42}$$

$$\Delta I^{dc}_{\mathfrak{l}} = \left|\Delta I^{dc}_{\mathfrak{l},1} \quad \cdots \Delta I^{dc}_{\mathfrak{l},\mathcal{H}}\right|^{\mathcal{T}} \tag{43}$$

$$\Delta\mathcal{V}^{dc}_{\mathfrak{l}} = \left|\Delta\mathcal{V}^{dc}_{\mathfrak{l},1} \quad \Delta\mathcal{V}^{dc}_{\mathfrak{l},2} \quad \cdots \Delta\mathcal{V}^{dc}_{\mathfrak{l},\mathcal{H}}\right|^{\mathcal{T}} \tag{44}$$

$$A_{I^{dc}_{\mathfrak{l}}} = \mathcal{d}\mathfrak{iag}\left\{\left[-\frac{\mathfrak{R}^{dc}_{\mathfrak{l},1}}{L^{dc}_{\mathfrak{l},1}} - \frac{\mathfrak{R}^{dc}_{\mathfrak{l},2}}{L^{dc}_{\mathfrak{l},2}} - \frac{\mathfrak{R}^{dc}_{\mathfrak{l},\mathcal{K}}}{L^{dc}_{\mathfrak{l},\mathcal{H}}}\right]\right\}$$

$$B_{I^{dc}_{\mathfrak{l}}\mathcal{V}^{dc}_{\mathfrak{l}}} = \mathcal{d}\mathfrak{iag}\left\{\left[-\frac{1}{L^{dc}_{\mathfrak{l},1}} - \frac{1}{L^{dc}_{\mathfrak{l},2}} - \frac{1}{L^{dc}_{\mathfrak{l},\mathcal{H}}}\right]\right\}$$

5.6. *DC-SMG Load*

DC load is displayed as a fixed resistance.

$$\mathfrak{R}^{dc}_{\mathfrak{lo},m} \qquad L^{dc}_{\mathfrak{l},} \qquad \mathfrak{R}^{dc}_{\mathfrak{l}} \tag{45}$$

$$\mathfrak{R}^{dc}_{\mathfrak{lo},\mathfrak{m}} = \frac{\left(\mathcal{V}^{dc,(0)}_{\mathfrak{bus},\mathfrak{m}}\right)^2}{\mathcal{P}^{dc,(0)}_{\mathfrak{lo},,\mathfrak{m}}}$$

The DC bus load is:

$$\mathcal{V}^{dc}_{\mathcal{b}\mathfrak{us},n} = \mathfrak{R}^{dc}_{\mathfrak{lo},\mathfrak{m}}\, I^{dc}_{\mathfrak{lo},\mathfrak{m}} \tag{46}$$

DC load state space model:

$$\Delta I^{dc}_{\mathfrak{lo}} = B^{dc}_{\mathfrak{lo}}\Delta\mathcal{V}^{dc}_{\mathfrak{bus}} \tag{47}$$

Where,

$$\Delta\mathcal{V}^{dc}_{\mathfrak{blus}} = \left|\Delta\mathcal{V}^{dc}_{\mathfrak{bus},1} \quad \Delta\mathcal{V}^{dc}_{\mathfrak{bus},2} \quad \cdots \Delta\mathcal{V}^{dc}_{\mathfrak{bus},N}\right|^{\mathcal{T}}$$

$$\Delta I^{dc}_{\mathfrak{lo}} = \left|\Delta I^{dc}_{\mathfrak{lo},1} \quad \Delta I^{dc}_{\mathfrak{lo},2} \quad \cdots \Delta I^{dc}_{\mathfrak{lo},\mathcal{N}}\right|^{\mathcal{T}}$$

$$B^{dc}_{\mathfrak{lo}} = \mathcal{d}\mathfrak{iag}\left\{\left[-\frac{1}{\mathfrak{R}^{dc}_{\mathfrak{lo},1}} - \frac{1}{\mathfrak{R}^{dc}_{\mathfrak{lo},2}} - \frac{1}{\mathfrak{R}^{dc}_{\mathfrak{lo},N}}\right]\right\}$$

Where, N is the number of DC buses

5.7. *DC-SMG Complete State Space Modeling*

The DC bus is neglected

$$\Delta\mathcal{V}^{dc}_{\mathcal{b}\mathfrak{us}} = \Delta\mathcal{V}_{con} \tag{48}$$

Voltage and/ or current laws are:

$$\Delta\mathcal{V}^{dc}_{\mathfrak{l}} = \mathcal{D}^{dc}_{\mathfrak{l},\mathfrak{bus}}\,\Delta\mathcal{V}^{dc}_{\mathcal{b}\mathfrak{us}} \tag{49}$$

$$\left(\mathcal{D}^{dc}_{\mathfrak{l},\mathfrak{bus}}\right)^{\mathcal{T}}\Delta I^{dc}_{\mathfrak{l}} + \Delta I^{dc}_{\mathfrak{lo}} - \Delta I^{dc}_{\mathrm{in}} = \Delta I_{\mathrm{con}}$$

$$\Delta\ I^{dc}_{\mathrm{in}} = \left|\Delta\ I^{\mathrm{dc}}_{\mathrm{in},1} \quad \Delta\ I^{\mathrm{dc}}_{\mathrm{in},2} \quad \cdots \Delta\ I^{\mathrm{dc}}_{\mathrm{in},N}\right|^{\mathcal{T}}$$

Wherever $\mathcal{D}^{dc}_{\mathfrak{l},\mathfrak{bus}}$ is the DC section line–bus incidence matrix.

DC section state space model is: -

$$X^{\cdot}_{\mathcal{DC}} = A_{\mathcal{DC}}\, X_{\mathcal{DC}} + B_{\mathcal{DC}}\,\Delta I^{dc}_{\mathrm{in}} \tag{50}$$

$$\mathrm{X}_{\mathcal{DC}} = \begin{bmatrix} \Delta\mathcal{V}_{\mathrm{con}} \\ \Delta\,\mathrm{I}_{\mathrm{l}}^{dc} \end{bmatrix}$$

$$\mathrm{B}_{\mathcal{DC}} = \begin{bmatrix} -\,\mathrm{B}_{\mathcal{V}_{\mathrm{con}}\mathrm{I}_{\mathrm{con}}} \\ 0 \end{bmatrix}$$

$$\mathrm{A}_{\mathcal{DC}} = \begin{bmatrix} \mathrm{A}_{\mathrm{cDn}} + \mathrm{B}_{\mathcal{V}_{\mathrm{con}}\mathrm{I}_{\mathrm{con}}}\mathrm{B}_{\mathrm{lo}}^{dc} & \mathrm{B}_{\mathcal{V}_{\mathrm{con}}\mathrm{I}_{\mathrm{cn}}}\left(\mathrm{D}_{\mathrm{l,bus}}^{dc}\right)^{\mathcal{T}} \\ \mathrm{B}_{\mathrm{I}_{\mathrm{l}}^{dc}\mathcal{V}_{\mathrm{l}}^{dc}}\,\mathrm{D}_{\mathrm{l,bus}}^{dc} & \mathrm{A}_{\mathrm{I}_{\mathrm{l}}^{dc}} \end{bmatrix}$$

6. ILC Section State Space Modeling

Swapping real Power between AC and DC:

$$\mathrm{P}_{\mathrm{exc,f}} = -\mathrm{P}_{ic,\mathrm{f}}^{\mathrm{ac}} = \mathrm{P}_{ic,\mathrm{f}}^{dc} \tag{51}$$

Real power transferred by every IC:

$$\Delta\,\mathrm{P}_{\mathrm{exc,f}} = -\mathrm{n}_{\mathcal{V},\mathrm{f}}\,\Delta\mathcal{V}_{ic,\mathrm{f}}^{dc} + \mathrm{n}_{\omega,\mathrm{f}}\,\Delta\omega_{ic,\mathrm{f}} \tag{52}$$

Real power flows from the AC sector to ILC:

$$\mathrm{P}_{ic,\mathrm{f}}^{\mathrm{ac}} = -\mathcal{V}_{ic,\mathrm{f}}^{\mathrm{ac}}\,\mathrm{I}_{in,\mathrm{f}}^{\mathrm{ic},d} \tag{53}$$

The inflow ILC current D–axis component:

$$\Delta\mathrm{I}_{in,\mathrm{f}}^{\mathrm{ic,d}} = \frac{1}{\mathcal{V}_{ic,\mathrm{f}}^{\mathrm{ac}(0)}}\,\Delta\,\mathrm{P}_{\mathrm{exc,f}} - \frac{\mathrm{P}_{\mathrm{exc,f}}^{(0)}}{\left(\mathcal{V}_{ic,\mathrm{f}}^{\mathrm{ac}(0)}\right)^2}\,\Delta\,\mathcal{V}_{ic,\mathrm{f}}^{\mathrm{ac}} \tag{54}$$

AC section reactive power using Q-V droop: -

$$\Delta\,\mathcal{Q}_{\mathrm{ic,f}} = \mathrm{n}_{\mathcal{Q},\mathrm{f}}\,\Delta\mathcal{V}_{\mathrm{ic,f}}^{\mathrm{ac}} \tag{55}$$

Reactive power from IC to AC section:

$$\mathcal{Q}_{\mathrm{ic,f}} = -\mathcal{V}_{\mathrm{ic,f}}^{\mathrm{ac}} \tag{56}$$

The inflow ILC current q-axis component:

$$\Delta\mathrm{I}_{in,\mathrm{f}}^{\mathrm{ic,q}} = -\frac{1}{\mathcal{V}_{ic,\mathrm{f}}^{\mathrm{ac}(0)}}\,\Delta\,\mathcal{Q}_{\mathrm{ic,f}} + \frac{\mathrm{Q}_{\mathrm{ic,f}}^{(0)}}{\left(\mathcal{V}_{ic,\mathrm{f}}^{\mathrm{ac}(0)}\right)^2}\,\Delta\,\mathcal{V}_{ic,\mathrm{f}}^{\mathrm{ac}} \tag{57}$$

Controlled IC current state space modeling:

$$\Delta\,\mathrm{I}_{in,\mathrm{f}}^{\mathrm{ic},dq} = \mathrm{C}_{\mathrm{I}_{\mathrm{inw}}^{\mathrm{ic}}}\Delta\omega_{\mathrm{f}} + \mathrm{C}_{\mathrm{I}_{\mathrm{in}}^{\mathrm{ic}}\mathcal{V}_{\mathrm{ic}}^{\mathrm{ac}}}\,\Delta\mathcal{V}_{\mathrm{ic}}^{\mathrm{ac}} + \mathrm{C}_{\mathrm{I}_{\mathrm{in}}^{\mathrm{ic}}\mathcal{V}_{\mathrm{ic}}^{dc}}\,\Delta\mathcal{V}_{\mathrm{ic}}^{dc} \tag{58}$$

$$\Delta\,\mathrm{I}_{in,\mathrm{f}}^{\mathrm{ic},dq} = \left|\Delta\,\mathrm{I}_{\mathrm{in},1}^{ic,\mathrm{d}}\,\Delta\,\mathrm{I}_{\mathrm{in},1}^{ic,q}\quad \Delta\,\mathrm{I}_{\mathrm{in},2}^{ic,\mathrm{d}}\quad \Delta\,\mathrm{I}_{\mathrm{in},2}^{ic,q}\cdots\Delta\,\mathrm{I}_{\mathrm{in,X}}^{ic,\mathrm{d}}\,\Delta\,\mathrm{I}_{\mathrm{in,X}}^{ic,q}\right|^{\mathcal{T}} \tag{59}$$

Where

$\Delta\mathcal{V}_{\mathrm{ic}}^{ac} = |\Delta\mathcal{V}_{\mathrm{ic},1}^{ac}\quad \Delta\mathcal{V}_{\mathrm{ic},2}^{ac}\quad \cdots\Delta\mathcal{V}_{\mathrm{ic,X}}^{ac}|^{\mathcal{T}}$,

$$\Delta\mathcal{V}_{\mathrm{ic}}^{dc} = \left|\Delta\mathcal{V}_{\mathrm{ic},1}^{dc}\quad \Delta\mathcal{V}_{\mathrm{ic},2}^{dc}\quad \cdots\Delta\mathcal{V}_{\mathrm{ic,X}}^{dc}\right|^{\mathcal{T}}$$

$$\mathcal{C}_{\mathrm{I}_{\mathrm{in}\omega}^{\mathrm{ic}}} = \left|\frac{\mathrm{n}_{\omega,1}}{\mathcal{V}_{ic,1}^{\mathrm{ac}(0)}}\quad 0\quad \frac{\mathrm{n}_{\omega,2}}{\mathcal{V}_{ic,2}^{\mathrm{ac}(0)}}\quad \frac{\mathrm{n}_{\omega,\mathcal{X}}}{\mathcal{V}_{ic,\mathrm{X}}^{\mathrm{ac}(0)}}\quad 0\right|^{\mathcal{T}}$$

Where,
X= number of ICs

$$\mathcal{C}_{\mathrm{I}_{\mathrm{in}}^{\mathrm{ic}}\mathcal{V}_{\mathrm{ic,f}}^{\mathrm{ac}}} = \left|\frac{\mathrm{P}_{\mathrm{excf}}^{(0)}}{\left(\mathcal{V}_{ic\mathrm{f}}^{\mathrm{ac}(0)}\right)^2}\quad \frac{-\mathrm{n}_{\mathcal{Q},\mathrm{f}}\,\Delta\mathcal{V}_{\mathrm{ic,f}}^{\mathrm{ac}(0)} + \mathcal{Q}_{\mathrm{ic,f}}}{\left(\mathcal{V}_{ic,\mathrm{f}}^{\mathrm{ac}(0)}\right)^2}\right|^{\mathcal{T}} \tag{60}$$

$$\mathcal{C}_{\mathrm{I}_{\mathrm{in}}^{\mathrm{ic}}\mathcal{V}_{\mathrm{ic,f}}^{dc}} = \left|\frac{\mathrm{n}_{\mathcal{V},\mathrm{f}}}{\mathcal{V}_{ic,\mathrm{f}}^{\mathrm{ac}(0)}}\quad 0\quad\right|^{\mathcal{T}} \tag{61}$$

Real power flows from the IC to the DC section:

$$\mathrm{P}_{ic,\mathrm{f}}^{dc} = \mathcal{V}_{ic,\mathrm{f}}^{dc}\,\mathrm{I}_{\mathrm{out,f}}^{\mathrm{ic}} \tag{62}$$

Out flow IC current: -

$$\Delta\mathrm{I}_{\mathrm{out,f}}^{\mathrm{ic}} = \frac{1}{\mathcal{V}_{ic,\mathrm{f}}^{dc(0)}}\,\Delta\,\mathrm{P}_{ic,\mathrm{f}}^{dc} - \frac{\mathrm{P}_{\mathrm{exc,f}}^{(0)}}{\left(\mathcal{V}_{ic,\mathrm{f}}^{dc(0)}\right)^2}\,\Delta\,\mathcal{V}_{ic,\mathrm{f}}^{dc} \tag{63}$$

The controlled outflow IC current state space model

$$\Delta\mathrm{I}_{\mathrm{out}}^{\mathrm{ic}} = \mathcal{C}_{\mathrm{I}_{\mathrm{out}\omega}^{\mathrm{ic}}}\Delta\omega_{\mathrm{f}} + \mathcal{C}_{\mathrm{I}_{\mathrm{out}}^{\mathrm{ic}}\mathcal{V}_{\mathrm{ic}}^{\mathrm{ac}}}\,\Delta\mathcal{V}_{\mathrm{ic}}^{dc} \tag{64}$$

$$\Delta\mathrm{I}_{\mathrm{out,f}}^{\mathrm{ic}} = \left|\Delta\mathrm{I}_{\mathrm{out},1}^{\mathrm{ic}}\quad \Delta\mathrm{I}_{\mathrm{out},2}^{\mathrm{ic}}\quad \cdots\Delta\mathrm{I}_{\mathrm{out,X}}^{\mathrm{ic}}\right|^{\mathcal{T}} \tag{65}$$

Where,

$$\mathcal{C}_{\mathrm{I}_{\mathrm{out}}^{\mathrm{ic}}\mathcal{V}_{\mathrm{ic}}^{\mathrm{ac}}} = diag\left\{\left[-\frac{\mathrm{n}_{\mathcal{V},1}\,\Delta\mathcal{V}_{\mathrm{ic},1}^{dc(0)} + \mathrm{P}_{exc,1}^{(0)}}{\left(\mathcal{V}_{ic,1}^{\mathrm{ac}(0)}\right)^2} - \frac{\mathrm{n}_{\mathcal{V},2}\,\Delta\mathcal{V}_{\mathrm{ic},2}^{dc(0)} + \mathrm{P}_{exc,2}^{(0)}}{\left(\mathcal{V}_{ic,2}^{dc(0)}\right)^2} - \frac{\mathrm{n}_{\mathcal{V},\mathrm{X}}\,\Delta\mathcal{V}_{\mathrm{ic,X}}^{dc(0)} + \mathrm{P}_{exc,\mathrm{X}}^{(0)}}{\left(\mathcal{V}_{ic,\mathrm{X}}^{dc(0)}\right)^2}\right]\right\},$$

$$\mathcal{C}_{\mathrm{I}_{\mathrm{in}\omega}^{\mathrm{ic}}} = \left|\frac{\mathrm{n}_{\omega,1}}{\mathcal{V}_{ic,1}^{dc(0)}}\quad \frac{\mathrm{n}_{\omega,2}}{\mathcal{V}_{ic,2}^{dc(0)}}\quad \frac{\mathrm{n}_{\omega,\mathrm{X}}}{\mathcal{V}_{ic,\mathcal{X}}^{dc(0)}}\quad\right|^{\mathcal{T}}$$

7. Complete State Space Modeling

The network operating frequency:

$$\omega_{\mathrm{ic,f}} = \omega_{\mathrm{c}} = \mathrm{D}_{\omega}\ \omega \tag{66}$$

The AC terminal voltage value of every ILC in the DQ frame:

$$\mathcal{V}_{\mathrm{ic,f}}^{\mathrm{ac}} = \mathcal{V}_{\mathrm{ic,f}}^{\mathrm{ac,D}}\ \cos\sigma_{\mathrm{f}} + \mathcal{V}_{\mathrm{ic,f}}^{\mathrm{ac,D}}\ \cos\sigma_{\mathrm{f}} \tag{67}$$

An angle amongst the local *D*-frame of the ILC and the common DQ frame reference is (σ_f).

State space modeling is:

$$\Delta\mathcal{V}_{\mathrm{ic}}^{\mathrm{ac}} = \mathcal{C}_{\mathrm{t}}^{\mathrm{ic}}\ \Delta\mathcal{V}_{\mathrm{ic}}^{\mathrm{ac},\mathrm{D}\mathcal{Q}} \tag{68}$$

Where,

$$\Delta\mathcal{V}_{\mathrm{ic}}^{\mathrm{ac,D}\mathcal{Q}} = \left|\ \Delta\mathcal{V}_{\mathrm{ic,1}}^{\mathrm{ac,D}}\ \ \Delta\mathcal{V}_{\mathrm{ic,1}}^{\mathrm{ac},\mathcal{Q}}\quad \Delta\mathcal{V}_{\mathrm{ic,2}}^{\mathrm{ac,D}}\quad \Delta\mathcal{V}_{\mathrm{ic,2}}^{\mathrm{ac},\mathcal{Q}} \cdots\ \Delta\mathcal{V}_{\mathrm{ic},\mathcal{X}}^{\mathrm{ac,D}}\ \ \Delta\mathcal{V}_{\mathrm{ic},\mathcal{X}}^{\mathrm{ac},\mathcal{Q}}\right|^{\mathcal{T}},$$

$$\mathcal{C}_{\mathrm{t,f}}^{\mathrm{ic}} = |\cos\Upsilon_0 \quad \sin\Upsilon_0|$$

The inflow ILC current in the DQ frame:

$$\mathrm{I}_{in,\mathrm{f}}^{\mathrm{ic,D}} = \mathrm{I}_{in,\mathrm{f}}^{\mathrm{ic},d} \cos\Upsilon_0 - \mathrm{I}_{in,\mathrm{f}}^{\mathrm{ic},q} \sin\Upsilon_0 \tag{69}$$

$$\mathrm{I}_{in,\mathrm{f}}^{\mathrm{ic},\mathcal{Q}} = \mathrm{I}_{in,\mathrm{f}}^{\mathrm{ic},q} \sin\Upsilon_0 + \mathrm{I}_{in,\mathrm{f}}^{\mathrm{ic},q} \cos\Upsilon_0 \tag{70}$$

$$\Delta\mathrm{I}_{\mathrm{ic}}^{\mathrm{ac,DQ}} = \mathcal{C}_{\mathrm{t}}^{\mathrm{ic}}\ \Delta\mathrm{I}_{\mathrm{ic}}^{\mathrm{ac},dq} \tag{71}$$

Where,

$$\Delta\mathrm{I}_{\mathrm{ic}}^{\mathrm{ac,D}\mathcal{Q}} = \left|\ \Delta\mathrm{I}_{\mathrm{ic,1}}^{\mathrm{ac,D}}\ \ \Delta\mathrm{I}_{\mathrm{ic,1}}^{\mathrm{ac,Q}}\quad \Delta\mathrm{I}_{\mathrm{ic,2}}^{\mathrm{ac,D}}\quad \Delta\mathrm{I}_{\mathrm{ic,2}}^{\mathrm{ac},\mathcal{Q}} \cdots\ \Delta\mathrm{I}_{\mathrm{ic},\mathcal{X}}^{\mathrm{ac,D}}\ \ \Delta\mathrm{I}_{\mathrm{ic},\mathcal{X}}^{\mathrm{ac,Q}}\right|^{\mathcal{T}},$$

$$\mathcal{C}_{\mathcal{T},\mathrm{f}}^{\mathrm{ic}} = \begin{vmatrix} \cos\Upsilon_0 & -\sin\Upsilon_0 \\ \sin\Upsilon_0 & \cos\Upsilon_0 \end{vmatrix}$$

A state space of the AC sector with AC terminals of ILCs:

$$\Delta\mathcal{V}_{\mathrm{ic}}^{\mathrm{ac,DQ}} = \mathcal{D}_{\mathrm{bus,ic}}^{\mathrm{ac}}\ \Delta\mathcal{V}_{\mathrm{bus}}^{\mathrm{ac}} \tag{72}$$

$$\Delta\mathrm{I}_{\mathrm{out}}^{ac} = \left(\mathcal{D}_{\mathrm{bus,ic}}^{\mathrm{ac}}\right)^{\mathcal{T}} \Delta\mathrm{I}_{\mathrm{in}}^{ic,\mathrm{DQ}} \tag{73}$$

Wherever $\mathcal{D}_{\mathrm{bus,ic}}^{\mathrm{ac}}$ *is* the incidence matrix links ILCs with AC buses:

The state space model after combining:

$$\Delta\mathcal{V}_{\mathrm{ic}}^{\mathrm{ac}} = \mathcal{C}_{\mathcal{T}}^{\mathrm{ic}}\,\mathcal{D}_{\mathrm{bus,ic}}^{\mathrm{ac}}\,\mathcal{C}_{\mathcal{T}}^{\mathrm{ac}}\ \Delta\mathcal{V}_{\mathrm{in}} + \mathcal{C}_{\mathcal{T}}^{\mathrm{ic}}\,\mathcal{D}_{\mathrm{bus,ic}}^{\mathrm{ac}}\ \mathcal{C}_{\ \mathcal{V}_{\mathrm{bus}\gamma}^{\mathrm{ac}}}\ \Delta\Upsilon \tag{74}$$

A state space links the DC sector with the DC terminals of ILCs:

$$\Delta\mathcal{V}_{\mathrm{ic}}^{dc} = \mathcal{D}_{\mathrm{bus,ic}}^{dc}\ \Delta\mathcal{V}_{\mathrm{bus}}^{dc} \tag{75}$$

$$\Delta\mathrm{I}_{\mathrm{in}}^{dc} = \left(\mathcal{D}_{\mathrm{bus,ic}}^{dc}\right)^{\mathcal{T}} \Delta\mathrm{I}_{\mathrm{out}}^{dc} \tag{76}$$

Where $\mathcal{D}_{\mathrm{bus,ic}}^{dc}$ *is* the incidence matrix relates ILCs with DC buses:

A state space model after merging:

$$\Delta\ \mathrm{I}_{\mathrm{out}}^{\mathrm{ac}} = \mathrm{C}_{\mathrm{AC-AC}}\ \Delta\mathrm{X}_{\mathrm{AC}} + \mathrm{C}_{\mathrm{AC}-\mathcal{D}\mathrm{C}}\ \Delta\mathrm{X}_{\mathcal{D}\mathrm{C}} \tag{77}$$

Where,

$$\mathrm{C}_{\mathrm{AC-AC}} = |\ \mathrm{C}_{\mathrm{AC-AC,1}}\ \ \mathrm{C}_{\mathrm{AC-AC,2}}\quad \mathrm{C}_{\mathrm{AC-AC,3}}\quad 0 \quad 0|$$

$$\mathrm{C}_{\mathrm{AC}-\mathcal{D}\mathrm{C}} = \left|\left(\mathcal{D}_{\mathrm{bus,ic}}^{\mathrm{ac}}\right)^{\mathcal{T}}\ \mathrm{C}_{\mathrm{t}}^{\mathrm{ic}}\ \mathrm{C}_{\mathrm{I}_{\mathrm{in}}^{\mathrm{ic}}\,\mathcal{V}_{\mathrm{ic}}^{dc}}\ \mathcal{D}_{\mathrm{bus,ic}}^{dc}\quad 0\ \right|$$

$$\mathrm{C}_{\mathrm{A}\mathcal{C}-\mathrm{A}\mathcal{C},1} = \left(\mathcal{D}_{\mathrm{bus,ic}}^{\mathrm{ac}}\right)^{\mathcal{T}}\ \mathrm{C}_{\mathrm{t}}^{\mathrm{ic}}\ \mathrm{C}_{\mathrm{I}_{\mathrm{in}}^{\mathrm{ic}}\,\mathcal{V}_{\mathrm{ic}}^{dc}}\ \ \mathrm{C}_{\mathcal{T}}^{\mathrm{ic}}\mathcal{D}_{\mathrm{bus,ic}}^{\mathrm{ac}}\ \mathcal{C}_{\mathcal{V}_{\mathrm{bus}\gamma}^{\mathrm{ac}}}$$

$$\mathrm{C}_{\mathrm{A}\mathcal{C}-\mathrm{A}\mathcal{C},2} = \left(\mathcal{D}_{\mathrm{bus,ic}}^{\mathrm{ac}}\right)^{\mathcal{T}}\ \mathrm{C}_{\mathrm{t}}^{\mathrm{ic}}\ \mathrm{C}_{\mathrm{I}_{\mathrm{in}}^{\mathrm{ic}}\,\omega}\ \mathrm{D}_{\omega}$$

$$\mathrm{C}_{\mathrm{A}\mathcal{C}-\mathrm{A}\mathcal{C},3} = \left(\mathcal{D}_{\mathrm{bus,ic}}^{\mathrm{ac}}\right)^{\mathcal{T}}\ \mathrm{C}_{\mathrm{t}}^{\mathrm{ic}}\ \mathcal{C}_{\mathrm{I}_{\mathrm{in}}^{\mathrm{ic}}\,\mathcal{V}_{\mathrm{ic}}^{dc}}\ \ \mathrm{C}_{\mathcal{T}}^{\mathrm{ic}}\ \mathcal{D}_{\mathrm{bus,ic}}^{\mathrm{ac}}\ \mathrm{C}_{\mathcal{T}}^{\mathrm{ac}}$$

$$\Delta\mathrm{I}_{\mathrm{in}}^{dc} = \mathcal{C}_{\mathcal{DC}-\mathrm{A}\mathcal{C}}\ \Delta\mathrm{X}_{\mathrm{A}\mathcal{C}} + \mathcal{C}_{\mathcal{DC}-\mathcal{DC}}\ \Delta\mathrm{X}_{\mathcal{DC}}$$

$$\mathcal{C}_{\mathcal{DC}-\mathrm{A}\mathcal{C}} = \left|0 \quad \left(\mathcal{D}_{\mathrm{bus,ic}}^{dc}\right)^{\mathcal{T}} \mathcal{C}_{\mathrm{I}_{\mathrm{in}}^{\mathrm{ic}}\,\omega}\ \mathcal{D}_{\omega}\quad 0 \quad 0 \quad 0\ \right|$$

$$\mathcal{C}_{\mathcal{DC}-\mathcal{DC}} = \left|\left(\mathcal{D}_{\mathrm{bus,ic}}^{dc}\right)^{\mathcal{T}}\ \mathcal{C}_{\mathrm{I}_{\mathrm{out}}^{\mathrm{ic}}\,\mathcal{V}_{\mathrm{ic}}^{dc}}\ \mathcal{D}_{\mathrm{bus,ic}}^{dc}\quad 0\ \right|$$

IOM- SMG state space model:

$$\mathrm{X}^{\cdot} = \mathrm{A}\cdot\mathrm{X} \tag{78}$$

Wherever the state vector of dimension X, the state matrix of size A:

$$\mathcal{X} = |(\mathcal{X}_{\mathcal{AC}})^{\mathcal{T}} \quad (\mathcal{X}_{\mathcal{AC}})^{\mathcal{T}}|^{\mathcal{T}}$$

$$\mathcal{A} = \begin{vmatrix} \mathcal{A}_{\mathcal{AC}} + \mathcal{B}_{\mathcal{AC}}\,\mathcal{C}_{\mathcal{AC}-\mathcal{AC}} & \mathcal{B}_{\mathcal{AC}}\,\mathcal{C}_{\mathcal{AC}-\mathcal{DC}} \\ \mathcal{B}_{\mathcal{DC}}\,\mathcal{C}_{\mathcal{DC}-\mathcal{AC}} & \mathcal{A}_{\mathcal{DC}} + \mathcal{B}_{\mathcal{DC}}\,\mathcal{C}_{\mathcal{DC}-\mathcal{DC}} \end{vmatrix}$$

8. Control of DGs in the H-SMG

There are two controllers of the DG unit, like primary and proposed controls. A primary control is based on the voltage, current, and droop control for power sharing. However, the proposed controller is used to develop the system frequency and perfect reactive power sharing. [37-40]

8.1. A Primary Control of AC-SMG

The primary droop controller constitutes the first stage of the inverter control architecture [8]. It regulates the output voltage and/or frequency in accordance with prevailing load conditions [41]. This controller operates by estimating the active and/or reactive power and applying appropriate droop coefficients to generate the corresponding voltage and/or frequency references [42]. Since droop control relies exclusively on locally measured variables for power sharing, it does not require a communication link among distributed units [37]. Figure 2 illustrates the overall control structure of the smart microgrid, which is implemented in the MATLAB/Simulink environment, as depicted in Figure 3. The power delivered at the inverter output terminals can be expressed by the following equations.

$$\tilde{\mathrm{p}} = \mathcal{V}_{\mathrm{od}}\imath_{\mathrm{od}} + \mathcal{V}_{\mathrm{oq}}\imath_{\mathrm{oq}} \tag{79}$$

$$\tilde{q} = -\mathcal{V}_{od}i_{od} + \mathcal{V}_{oq}i_{oq} \tag{80}$$

Wherever i_{od} , $\mathcal{V}_{\circ d}$ are d-axis for current and voltage, and i_{oq} , $\mathcal{V}_{oq}$ are $q-$ axis for current and voltage, ω_c is a pass filter cut-off frequency utilized in surveys:

$$P = \frac{\omega_c}{s+\omega_c}\widetilde{P} \tag{81}$$

$$Q = \frac{\omega_c}{s+\omega_c}\tilde{q} \tag{82}$$

The droop coefficients m_p, n_q indicate the *f*-P drooping behavior, the V-Q droop behavior. A droop control for the VCM or CCM is displayed as: [7, 42]

$$\omega_n = \omega_n^* - m_p\, P_n \tag{83}$$

$$n_{od}^{n} = \mathcal{V}_{od}^* - n_q\, Q_n \tag{84}$$

$$\mathcal{V}_{oq}^{n} = 0 \tag{85}$$

The droop coefficient n_q and m_p are computing as:

$$m_p = \frac{\omega_{max} - \omega_{min}}{P_{max}} \tag{86}$$

$$n_q = \frac{\mathcal{V}_{max} - \mathcal{V}_{min}}{Q_{max}} \tag{87}$$

Wherever K_{dp} , K_{dq}, ω_n^* , $\mathcal{V}_n$, $and\ \omega_n$, P_n, Q_n are droop coefficients, frequency, voltage, and new frequency, active and reactive power, and $\mathcal{V}_{od}^*$, $\mathcal{V}_{oq}^*$ are the d-axis, q–axis voltage reference, respectively.

VCM differential-algebraic equations are: [43]

$$\emptyset_{dn} = \mathcal{V}_{odn}^* - \mathcal{V}_{odn}^{n} \tag{88}$$

$$\emptyset_{qn} = \mathcal{V}_{oqn}^* - \mathcal{V}_{dqn}^{n} \tag{89}$$

$$i_{dn}^* = F_n i_{odn} - \omega_s\, C_{nF}\mathcal{V}_{oqn} + K_{pvn}\ (\mathcal{V}_{od}^* - \mathcal{V}_{od}^{n}) + K_{Ivn}\ \emptyset_{dn} \tag{90}$$

$$i_{qn}^* = F_n i_{oqn} - \omega_s\, C_{nF}\mathcal{V}_{odn} + K_{pvn}\ \left(\mathcal{V}_{oq}^* - \mathcal{V}_{oq}^{n}\right) + K_{Ivn}\ \emptyset_{qn} \tag{91}$$

Where $\mathcal{V}_{odn}$,$\mathcal{V}_{oqn}$, i_{odn} and i_{oqn} are the *dq*-component of $\mathcal{V}_{on}$ $and\ i_{on}$, ω_s the nominal frequency, and the variables of the PI controller are $\emptyset_{dn}, \emptyset_{qn}$.

CCM differential-algebraic equations are: [43]

$$\gamma_{dn} = i_{dn}^* - i_{dn}^{n} \tag{92}$$

$$\gamma_{qn} = i_{qn}^* - i_{qn}^{n} \tag{93}$$

$$\mathcal{V}_{dn}^* - \omega_s\, L_{nF}\mathcal{V}_{qn} + K_{prn}\ (i_{dn}^* - i_{dn}) + K_{Icn}\,\gamma_{dn} \tag{94}$$

$$\mathcal{V}_{qn}^* = \omega_s\, L_{nF} i_{dn} + K_{pcn}\ \left(i_{qn}^* - i_{qn}^{n}\right) + K_{Icn}\,\gamma_{qn} \tag{95}$$

Where γ_{dn} , $and\ \gamma_{qn}$ are the new PI controller auxiliary states. LCL filter displayed as: [40]

$$\dot{i}_{d}^{n} = -\left(\Re_{fn}/L_{fn}\right) i_{d}^{n} + \omega i_{q}^{n} - \left(1/L_{fn}\right)\mathcal{V}_{\circ d}^{n} + \left(1/L_{fn}\right)\mathcal{E}_{d}^{n} - i_{q0}^{n}\,\omega_n \tag{96}$$

$$\dot{i}_{q}^{n} = -\omega i_{d}^{n} - \left(\Re_{fn}/L_{fn}\right) i_{q}^{n} - \left(1/L_{fn}\right)\mathcal{V}_{oq}^{n} + \left(1/L_{fn}\right)\mathcal{E}_{q}^{n} - i_{d0}^{n}\,\omega_n \tag{97}$$

$$\dot{\mathcal{V}}_{od}^{n} = -\left(1/C_{fn}\right) i_{d}^{n} + \omega\mathcal{V}_{oq}^{n} - \left(1/C_{fn}\right)i_{od}^{n} + \mathcal{V}_{oq0}^{n}\omega_n \tag{98}$$

$$\dot{\mathcal{V}}_{oq}^{n} = \left(1/C_{fn}\right)i_{q}^{n} - \omega\mathcal{V}_{oq}^{n} - \left(1/C_{fn}\right)i_{oq}^{n} - \mathcal{V}_{od0}^{n}\omega_n \tag{99}$$

$$\dot{i}_{od}^{n} = -\left(\Re_{i}^{\ n}/L_{i}^{\ n}\right) i_{od}^{n} + \omega i_{oq}^{n} - \left(1/L^{n}{}_{i}\right)\mathcal{V}_{od}^{n} - \left(1/L^{n}{}_{i}\right)\mathcal{V}_{pcc\cdot d}^{n} + i_{oq0}^{n}\omega^{n}{}_{c} \tag{100}$$

$$\dot{i}_{oq}^{n} = -\omega i_{od}^{n} - \left(\Re_{i}^{\ n}/L_{i}^{\ n}\right) i_{oq}^{n} + \left(1/L^{n}{}_{i}\right)\mathcal{V}_{oq}^{n} - \left(1/L^{n}{}_{i}\right)\mathcal{V}_{pcc\cdot q}^{n} - i_{od0}^{n}\omega^{n}{}_{c} \tag{101}$$

8.2. Voltage / Current Control

Proportional–Integral (PI) controllers are widely employed in voltage regulation loops to minimize steady-state errors while maintaining system stability and robustness. In decentralized control architectures, PI regulators are used to generate the reference current or voltage signals.

The PI control structure is well established and typically incorporates decoupling and feedforward control loops to enhance dynamic performance.

The dynamic behavior of the voltage control loop can be described by the following relations:

$$i_d^* = K_{pv}(\mathcal{V}_{od}^* - \mathcal{V}_{\circ d}) + K_{pv}\int(\mathcal{V}_{od}^* - \mathcal{V}_{\circ d})\,dt - \omega^* C_f\,\mathcal{V}_{oq} + \mathcal{F} i_{od} \tag{102}$$

$$i_q^* = K_{pv}\left(\mathcal{V}_{oq}^* - \mathcal{V}_{oq}\right) + K_{iv}\int\left(\mathcal{V}_{oq}^* - \mathcal{V}_{oq}\right)dt - \omega^* C_f\,\mathcal{V}_{od} + \mathcal{F} i_{oq} \tag{103}$$

Where proportional gain is K_{pv}, K_{iv} is integral gain, C_f is filter capacitance, feed forward gain is $\mathcal{F}$.

The voltage across the filter inductor dynamics is specified as:

$$\mathcal{V}_d^* = K_{pi}(i_d^* - i_d) + K_{ii}\int (i_d^* - i_d)\, dt - \omega^* L_f\, i_q + \mathcal{V}_{od} \quad (104)$$

$$\mathcal{V}_q^* = K_{pi}(i_q^* - i_q) + K_{ii}\int (i_d^* - i_q)\, dt - \omega^* L_f\, i_d + \mathcal{V}_{oq} \quad (105)$$

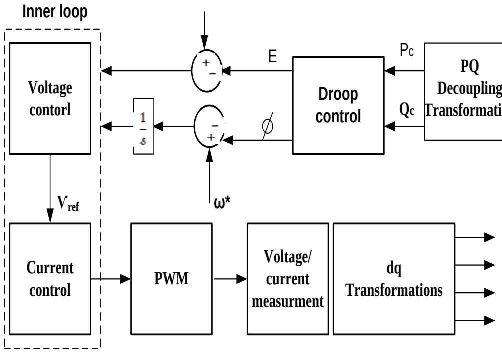

Fig. 2 Control cascade of SMG

In hybrid smart microgrids, the dynamic response to load variations is often delayed due to the low-frequency regulation mechanisms that govern inverter voltage through the Q–V droop characteristic and control reactive power based on voltage deviations from the reference value. To address this limitation, the droop control structure is augmented with an additional control stage comprising a gain block and an integral lead compensator, which is activated when the inverter output voltage exceeds the voltage at the point of common coupling. The proposed controller generates a compensating signal that mitigates frequency anomalies by offsetting the delay introduced by the low-pass filter [44]. The controller design is based on the deviation of the delay angle at higher droop gain values (m_p), as illustrated in Figure 4. The complete implementation of the proposed adaptive droop controller is realized in the MATLAB/Simulink environment, as shown in Figure 5. The controller gain K is intended as the magnitude of frequency drop $\Delta\omega = -m_p P$ equivalents the compensator drop ($\Delta\omega_{pss}$) in Figure 3. The following mathematical state–space model, which presents a single inverter unit,

$$\frac{d}{dt}\begin{vmatrix}\Delta\delta\\ \Delta P\\ \Delta Q\end{vmatrix} = A_P\begin{vmatrix}\Delta\delta\\ \Delta P\\ \Delta Q\end{vmatrix} + B_{P\omega_{ref}}|\Delta\omega_{ref}| + B_P\,\Delta F_{iv} \quad (106)$$

Wherever

$$\Delta F_{iv} = |\,\Delta i_{id} \quad \Delta i_{iq} \quad \Delta v_{od} \quad \Delta v_{oq} \quad \Delta i_{od} \quad \Delta i_{oq}\,|^{T}$$

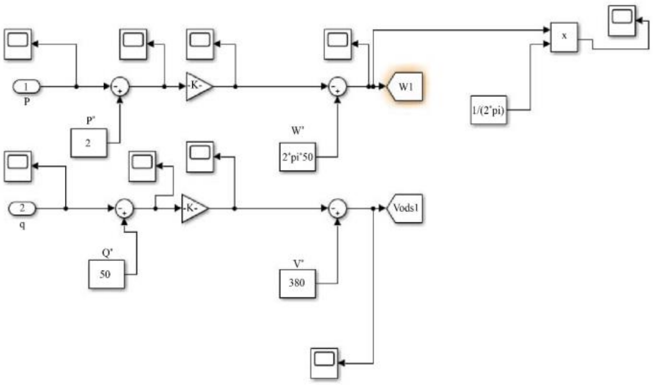

(a) Droop controller

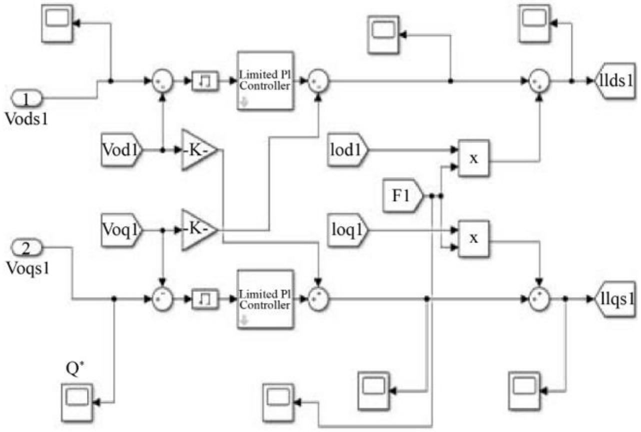

(b) Voltage controller

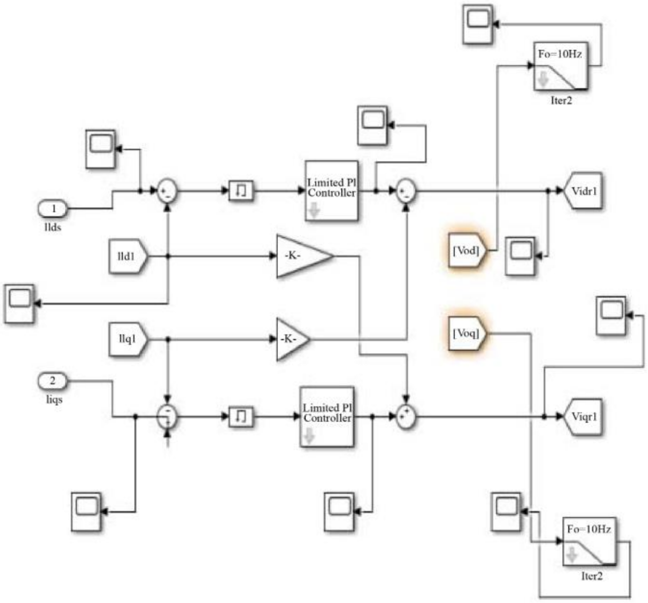

(c) Current control

Fig. 3 Cascaded controller procedure for the inverter from Matlab Simulink

Wherever the linearized equations matrix coefficients are Ap and Bp, ω_{ref} the input frequency of the system, and ΔF_{iv} is the disturbance.

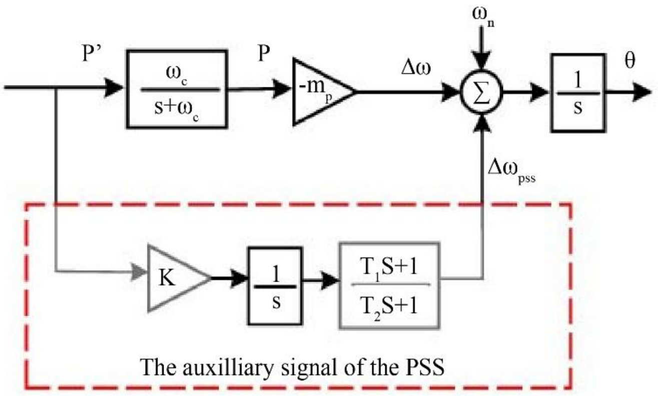

Fig. 4 Design technique of the proposed control signal [45]

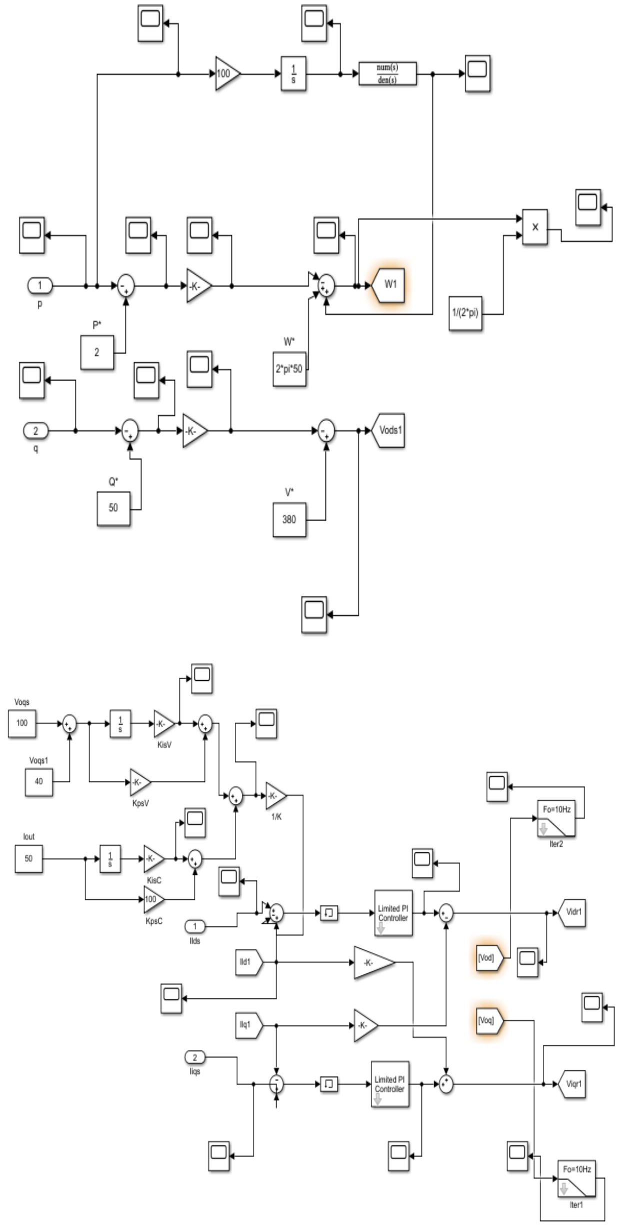

Fig. 5 A proposed droop control in Matlab Simulink

The predictable state–space model ($\Delta\omega_{pss}$):

$$\Delta\omega_{pss} = P` * K\left(\frac{s\,\mathcal{T}_1+1}{s\,\mathcal{T}_2+1}\right) \tag{107}$$

The Pss output is a function of the input f_{ini} and a set of parameters K, $\mathcal{T}_1$, and $\mathcal{T}_2$. Pss output is utilized to normalize the output frequency of inverter units. The $\Delta\acute{\omega}_{pss}$ new state–space model is:

$$\Delta\acute{\omega}_{pss}=\Delta\omega_{pss}\left(\frac{-1}{\mathcal{T}_2}\right)+ F_{ini}\Delta f_{if}\left(\frac{K}{\mathcal{T}_2}\right)+F_{ini}\frac{d}{dt}\,\Delta F_{if}\left(\frac{K,\mathcal{T}_1}{\mathcal{T}_2}\right) \tag{108}$$

Consequently, the first state Δδ will be changed according to the novel control as:

$$\Delta\,\omega = -\,\mathcal{m}_{\mathcal{p}}\,P - \Delta\,\omega_{pss} \tag{109}$$

$$\Delta\,\dot{\delta} =-\,\mathcal{m}_{\mathcal{p}}\,P - \Delta\,\omega_{pss} - \Delta\,\omega_{ref} \tag{110}$$

The modified system's state–space is:

$$\Delta\,\dot{X}_P = A_p\Delta\,X_P + B_{Pref}\,\Delta\omega_{ref} + B_{P1}\Delta\,F_{iv} + B_{P2}\frac{d}{dt}\,\Delta\,F_{iv}, \tag{111}$$

$$\Delta\,X_P = |\Delta\delta \quad \Delta P \quad \Delta Q \quad \Delta\omega_{pss}|^{\mathcal{T}} \tag{112}$$

Wherever $\Delta\,X_P$ is the phase angle deviation, A_p, B_{Pref}, B_{P1}, and B_{P2} signifies the coefficients of linearized equations, B_{Pref} and B_{P1} are a function of the input $\Delta\,\omega_{ref}$, ΔF_{iv} is the disturbance, and B_{P2} is the time derivative function of the disturbance $\frac{d}{dt}\,F_{iv}$. A state–space model can be used to design a controller system that regulates the inverter's voltage and frequency.

9. Results of the Simulation

The proposed controller is implemented and evaluated in the MATLAB/Simulink environment. This section presents a comparative analysis between the conventional droop control method and the proposed adaptive strategy to assess the validity of the developed approach. The primary objective of this comparison is to demonstrate the superior performance of the controller in achieving stable and equitable power sharing while mitigating voltage and current deviations under three operating scenarios: steady-state conditions, load disconnection (reduction in load demand), and load increase. Furthermore, the proposed control strategy enhances power quality in hybrid smart microgrids by improving AC frequency and DC voltage regulation, while maintaining accurate power exchange between the interconnected smart microgrids. By reinforcing the performance of the primary control layer, the adaptive approach ensures system stability across a wide range of droop coefficient values, thereby offering greater robustness.

9.1. Case (1) Steady State Case Operation

This scenario considers an islanded operation of the hybrid smart microgrid, supplying three distinct loads. The steady-state condition represents the normal operating mode of the H-SMG, during which the waveform profiles of the three loads are examined. Under conventional primary droop control, deviations in the voltage–frequency waveforms of the smart microgrid cannot be fully compensated, leading to mismatches in active and/or reactive power sharing among the associated distributed generators. With the implementation of the proposed control strategy, these deviations are effectively corrected, resulting in balanced power sharing among the distributed generators during steady-state operation, as illustrated in Figures 6-18.

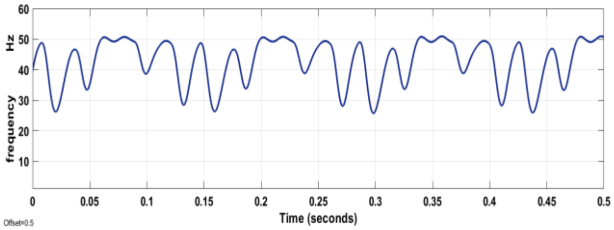

(a) Primary control

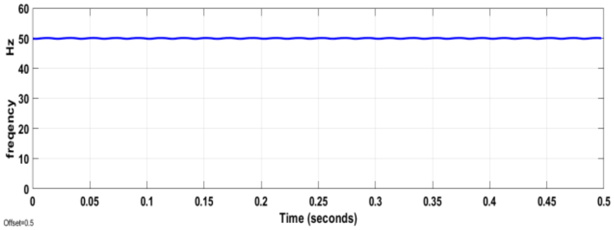

(b) Proposed control

Fig. 6 Comparison of frequency values in case (1)

Table 2. The test parameters

Parameter	Notation	Value
Vwind1	Wind voltage	440 V
Vwind2	Wind voltage	440 V
Vpv1	PV voltage	666 V
Vpv2	PV voltage	666 V
Vdc	DC voltage	700 V
ω	Nominal Frequency	50 Hz
Load power	P1,P2,P2	50,10,40 Kw
$\boldsymbol{\omega_c}$	Cut-off frequency of a low-pass filter	3.14 rad/s
$\boldsymbol{\mathcal{K}_{psc}}$	Voltage controller P gain	0.168
$\boldsymbol{\mathcal{K}_{isv}}$	Voltage controller, I gain	189.3
$\boldsymbol{\mathcal{K}_{isc}}$	Current controller P gain	13.37
$\boldsymbol{\mathcal{K}_{psi}}$	Current controller I gain	1005.3
$\mathbf{m_p}$ and $\mathbf{n_q}$	Droop coefficients	2.4 $*10^{-4}$, 10$*10^{-4}$
Cf	Filter capacitance	11 F

Figure 6 illustrates a comparison of the system frequency response obtained using the conventional primary controller and the proposed droop controller over the time range from t = 0 s to t = 0.5 s. With the primary controller, the frequency exhibits significant oscillations ranging from 27 Hz to 50.2 Hz, and then transitions to an oscillatory waveform centered around 51.7 Hz. In contrast, the proposed adaptive controller achieves a steady-state frequency of 50.13 Hz Figures 7-8, Compare the active power (Pload) and reactive power (Qload) of the load under both control strategies starting from t= 0 s until t= 0.5 s. As shown in Figure 7, Pload displays oscillatory behavior between 17, 80 W and 23,760 W when the primary controller is used. In comparison, the proposed adaptive controller smoothly adjusted to a steady value of 12,520 W. In Figure 8, Qload oscillates between 745 Var and 7,028 Var under the primary controller. The proposed adaptive controller gives a steady value of 49, 83 Var. Figures 9-14 present a comparative analysis of the voltage and current waveforms for the three loads, namely (Vload1, Vload2, Vload3), as well as (Iload1, Iload2, Iload3), under the conventional droop control and the proposed adaptive control schemes over the time interval from t = 0 s to t = 0.5 s. Variations in load demand result in corresponding changes in voltage and current magnitudes, leading to increased waveform distortion under these operating conditions.

As shown in Figure 9, the voltage of load 1 (Vload1) exhibits significant oscillations ranging from 76 V to 275 V when regulated by the conventional primary controller. In contrast, the proposed adaptive controller stabilizes Vload1 at approximately 335 V. Figure 10 indicates that the current of load 1 (Iload1) fluctuates between 34 A and 105 A under primary droop control, whereas it smoothly converges to a steady-state value of 89 A when the proposed controller is applied. Similarly, Figure 11 shows that Vload2 varies between 90 V and 276 V with the primary controller, while the proposed adaptive strategy maintains a stable voltage of 238 V. As illustrated in Figure 12, the current of load 2 (Iload2) oscillates within the range of 7.5 A to 19.5 A under conventional control; however, it reaches a steady-state value of 17 A under the proposed control scheme.

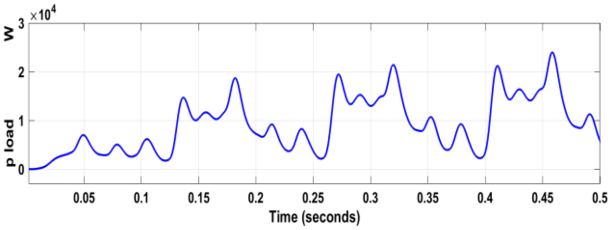

(a) Primary control

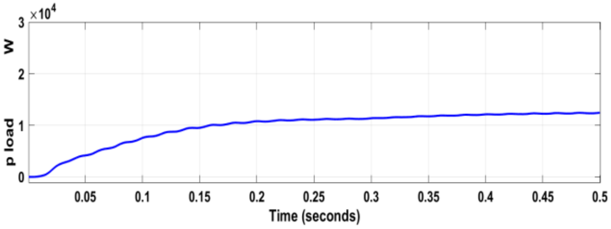

(b) Proposed control

Fig. (7) load active power in case (1).

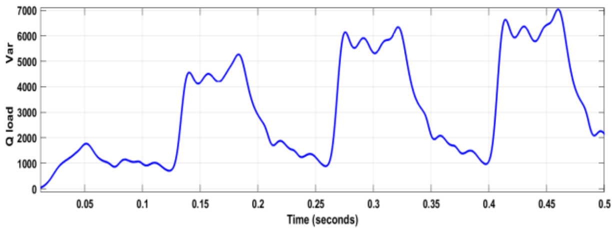

(a) Primary control

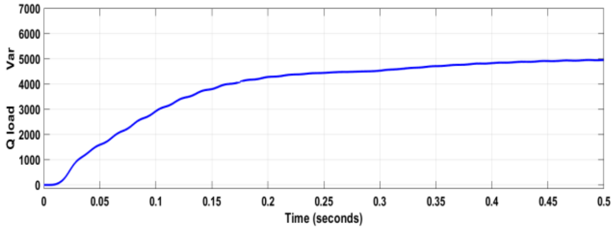

(b) Proposed control

Fig. 8 load reactive power in case (1)

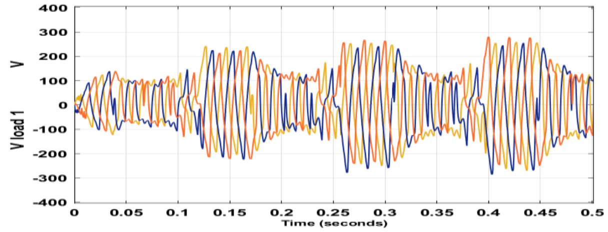

(a) Primary controller

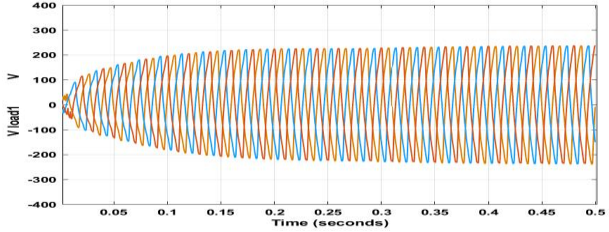

(b) Proposed control

Fig. 9 Comparison of Vload1 in case (a)

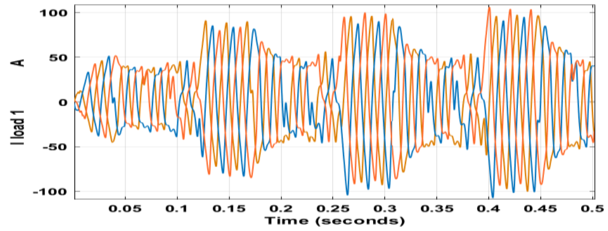

(a) Primary control

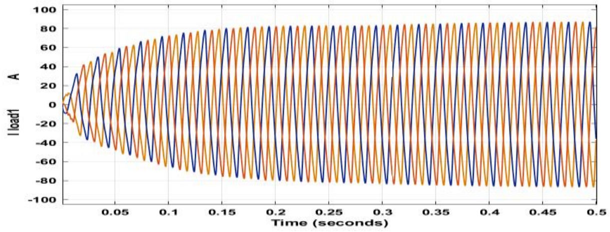

(b) Proposed control

Fig. 10 Comparison of Iload1 in case (1)

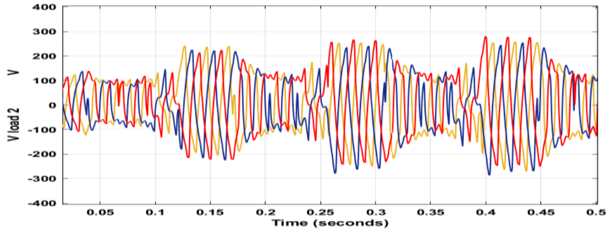

(a) Primary control

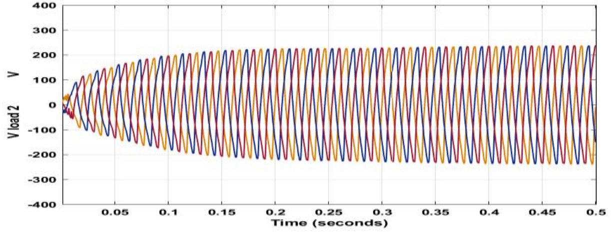

(b) Proposed control

Fig. 11 Vload2 output in case (1)

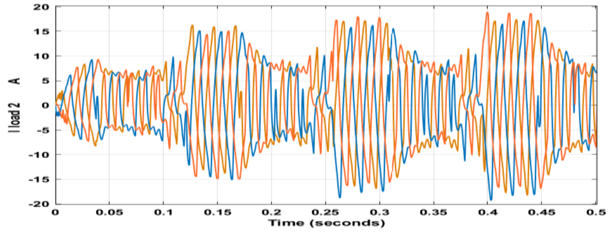

(a) Primary controller

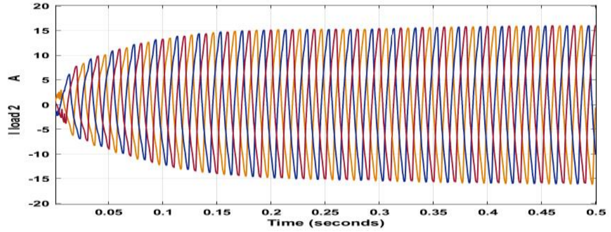

(b) Proposed controller

Fig. 12 Iload2 output in case (1)

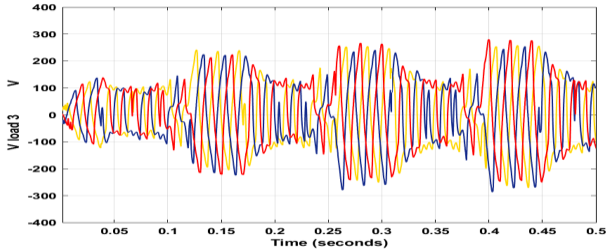

(a) Primary control

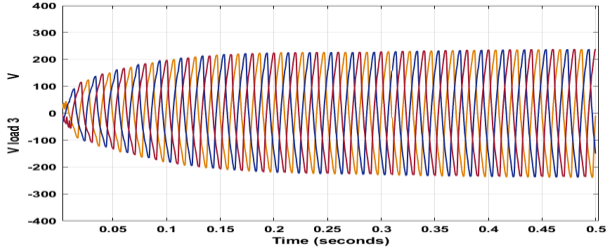

(b) Proposed controller

Fig. 13 Vload3 in case (1)

For load 3, Figure 13 demonstrates that Vload3 fluctuates between 84 V and 275.9 V when controlled by the primary droop method. The proposed controller significantly improves voltage regulation, maintaining Vload3 at approximately 237.5 V. Correspondingly, Figure 14 shows that Iload3 oscillates between 32 A and 76 A under primary control, whereas the proposed adaptive controller regulates the current to a stable value of 64 A. Overall, the proposed control approach produces voltage and current waveforms that are nearly sinusoidal with reduced distortion and improved steadiness compared to the conventional control case. Figures 15-16, compare the performance of the two controllers in regulating Pdroop and Qdroop under two scenarios. In Figure 15, Pdroop exhibits oscillatory behavior ranging from 6,890 W to 22,950W under the primary controller. In contrast, with the proposed adaptive controller, Pdroop maintains a steady-state value of 28,052 W. Figure 16 shows that Qdroop oscillates between 17,810 Var and 39,880 Var when using the primary controller. Under the proposed controller, Qdroop maintains a steady-state value of 27,020 Var.

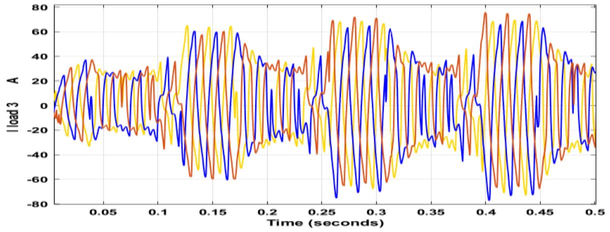

(a) Primary control

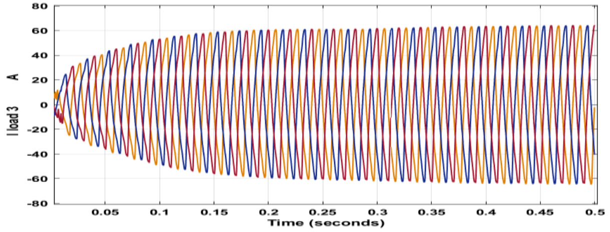

(b) Proposed control
Fig. 14 Iload3 in case (1)

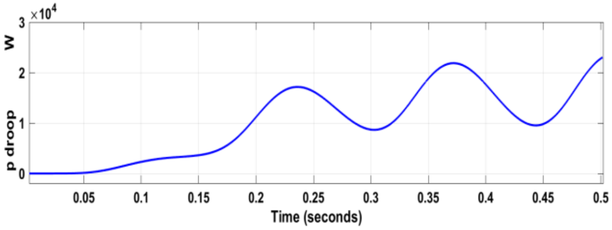

(a) Primary controller

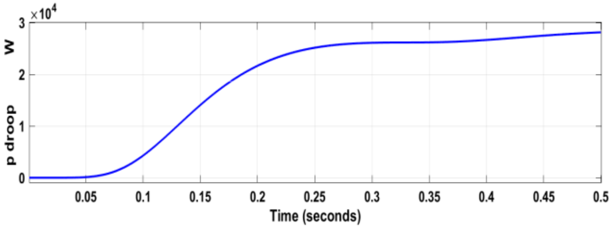

(b) Proposed control
Fig. (15) Droop active power outputs in case (1)

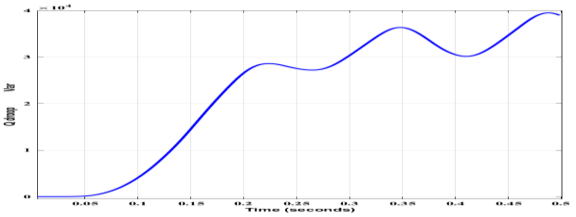

(a) Primary controller

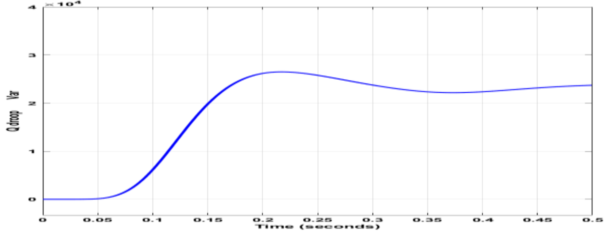

(b) Proposed controller
Fig. 16 Droop reactive power output in case (1)

Figures 17-18 present a comparison of inverter output voltage and DC bus voltage (Vdc), respectively, under both control strategies. Figure 17: The inverter output oscillates between 64 V and 175 V with the primary controller. With the proposed controller, the inverter output maintains a steady-state value of 159 V. In Figure 18, Vdc fluctuates between 485 V and 667 V with the primary controller. Under the proposed adaptive controller, Vdc has a steady-state value of 453V. It can be realized that in case (b), under the proposed controller, the inverter output and Vdc are better than in case (a).

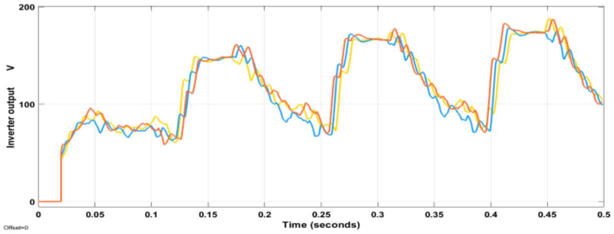

(a) Primary controller

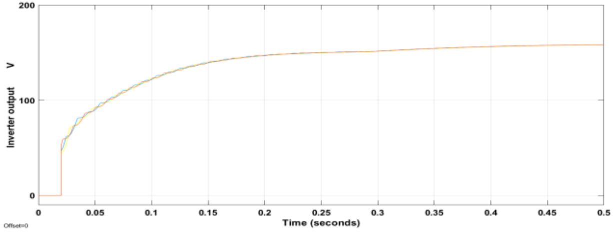

(b) Proposed controller
Fig. 17 Inverter output in case (1).

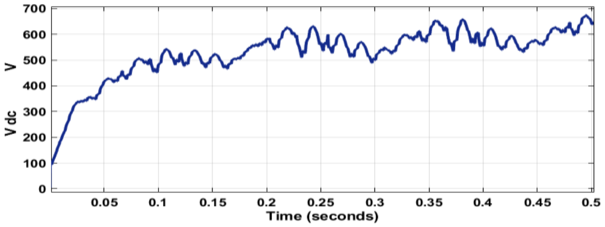

(a) Primary controller

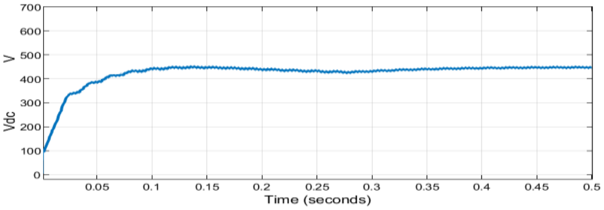

(b) Proposed control

Fig. 18 Vdc output in case (1)

9.2. Case (2) Interruption of one Load from Service (Reducing the Load)

This operating scenario examines a hybrid smart microgrid when loads 1 and 2 are connected, while load 3 remains disconnected with its switch initially open. Under the adaptive control strategy, oscillations in the smart microgrid voltage–frequency waveforms are effectively mitigated, resulting in improved regulation of frequency, voltage, active power, and reactive power. Moreover, the proposed controller ensures balanced power sharing among the distributed generators during steady-state operation, as illustrated in Figures 19-30. Figure 19 compares the frequency responses obtained using the conventional primary droop controller and the proposed adaptive droop controller over the interval from t = 0 s to t = 0.5 s. When the primary controller is applied, the system frequency exhibits pronounced oscillations ranging from 29 Hz to 50.2 Hz. In contrast, the proposed adaptive controller maintains the frequency close to its nominal value, stabilizing it at approximately 50.15 Hz. Figures 20-21, compare the Pload and Qload of the load under both control strategies. As given in Figure 20, Pload displays oscillatory behavior between 2,207 W and 22,762 W when the primary controller is used. In comparison, the proposed adaptive controller adjusted to a steady value of 21,724 W. In Figure 21, Qload oscillates between 745 Var and 7,028 Var under the primary controller. With the proposed adaptive controller, adjusted to the steady state value of 8633 Var. Figures 22-27 illustrate the comparison for Vload1, Vload2, Vload3, and Iload1, Iload2, Iload3 waveforms for the three loads under two control approaches. In Figure 22, Vload1 oscillates between 91.6V and 314.8V when using a primary controller. With the proposed controller, Vload1 is stabilizing at a steady-state value of 315V. Figure 23 shows that Iload1 oscillates between 32.7 A and 115.6 A when controlled by the primary controller. In contrast, under the proposed controller, Iload1 holds smoothly to a steady-state value of 115.7 A.

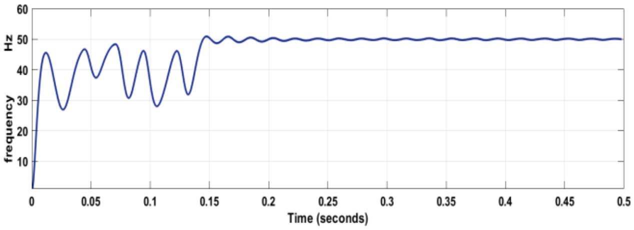

(a) Primary control

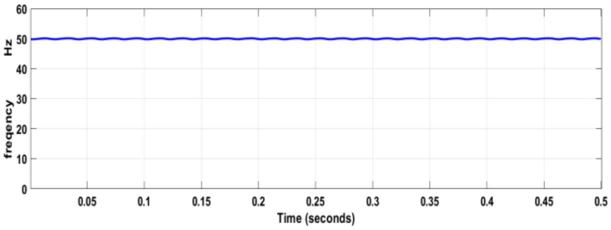

(b) Proposed control

Fig. 19 Frequency in case (2)

In Figure 24, Vload2 fluctuates between 94.5 V and 313.8 V under the primary controller. The proposed controller maintains Vload2 at a steady-state value of 314V. Figure 25 shows that Iload2 oscillates between 7 A and 21.5 A with the primary controller. Under the proposed controller, Iload2 has a steady-state value of 21.6 A. In Figure 26, Vload3 varies between 96 V and 312.5 V with the primary controller. The proposed controller achieves a steadier performance, maintaining Vload3 at 313V.

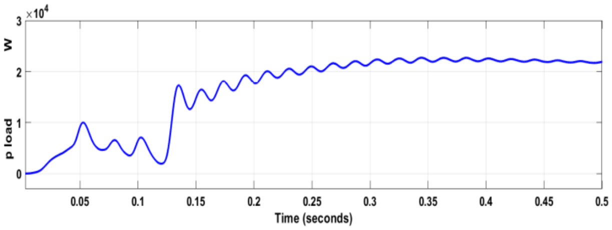

(a) Primary control

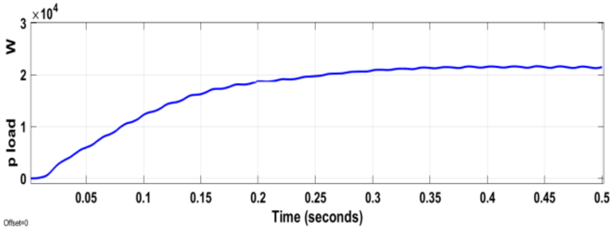

(b) Proposed control

Fig. 20 Load active power in case (2)

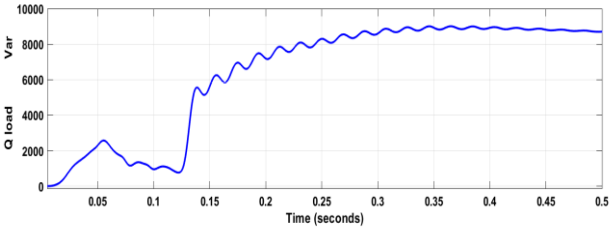

(a) Primary control

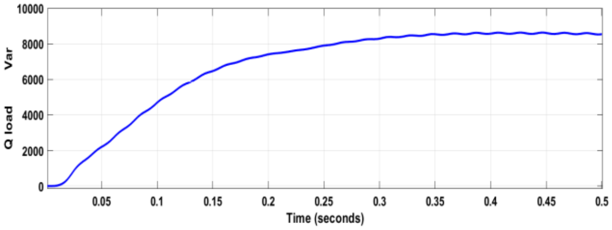

(b) Proposed control

Fig. 21 Load reactive power output in case (2)

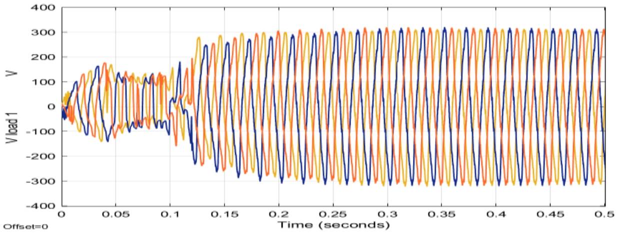

(a) Primary controller

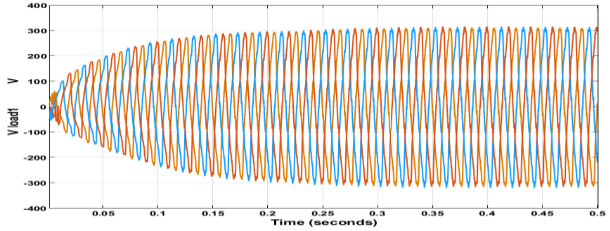

(b) Proposed control

Fig. 22 VLoad1 in case (2).

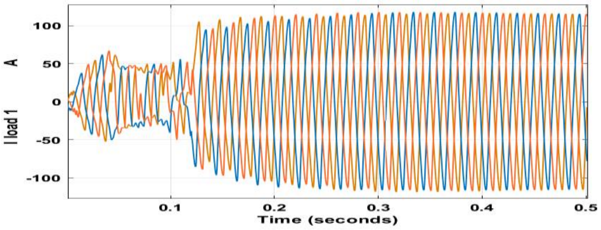

(a) Primary controller

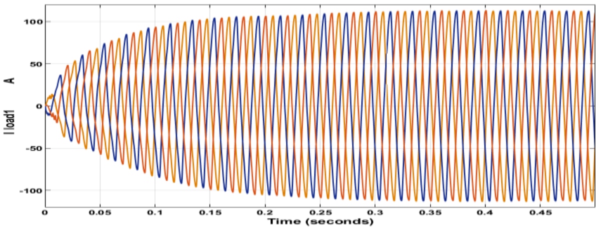

(b) Proposed control

Fig. 23 Iload1 output in case (2).

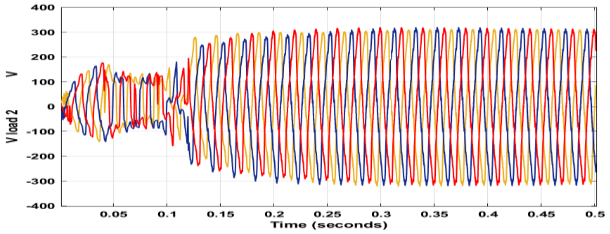

(a) Primary control

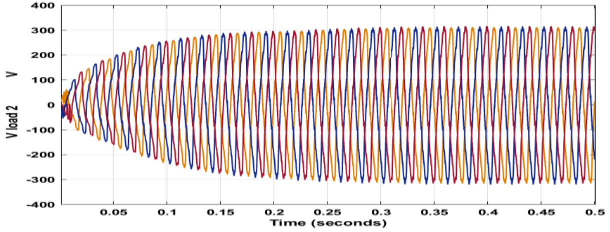

(b) Proposed control

Fig. 24 Comparison of Vload 2 output in case (2).

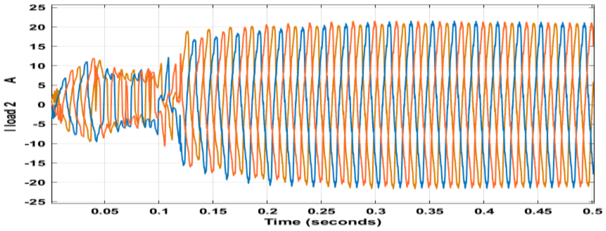

(a) Primary controller

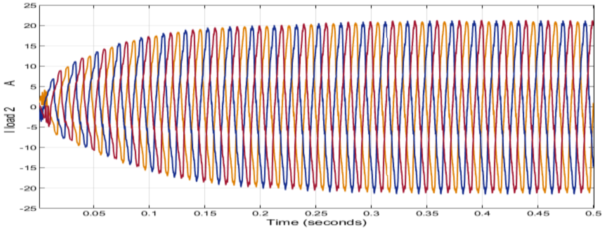

(b) Proposed control

Fig. 25 Iload2 wave in case (2).

Finally, Figure 27 shows that Iload3 is 0 A under the primary controller. The proposed adaptive controller regulates Iload3 to 0 A. It is realized under the proposed controller; the voltage and current values are pure sinusoidal waves, and the values are greater than those in case (a).

Figures 28-29, compare the performance of the two controllers in regulating Pdroop and Qdroop under two scenarios. In Figure 28, Pdroop exhibits oscillatory behavior ranging from 2,299 W to 32,170 W under the primary controller.

In contrast, with the proposed adaptive controller, Pdroop is adjusted to a steady-state value of 28,770 W. Figure 29 shows that Qdroop oscillates between 3,921 Var and 24,457 Var when using the primary controller. Under the proposed controller, Qdroop is adjusted to a steady-state value of 16,550 Var.

Figures 30 - 31 illustrate a comparison of the inverter output voltage waveform and Vdc, respectively, under the conventional primary droop controller and the proposed adaptive control strategy. As shown in Figure 30, the inverter output voltage exhibits substantial oscillations ranging from 75 V to 214 V when regulated by the primary controller. In contrast, the proposed adaptive controller stabilizes the inverter output at a steady-state value of approximately 207.5 V.

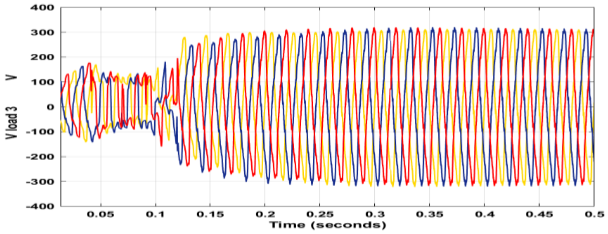

(a) Primary controller

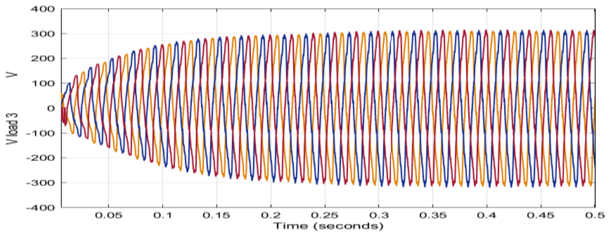

(b) Proposed control

Fig. 26 Vload3 wave in case (2)

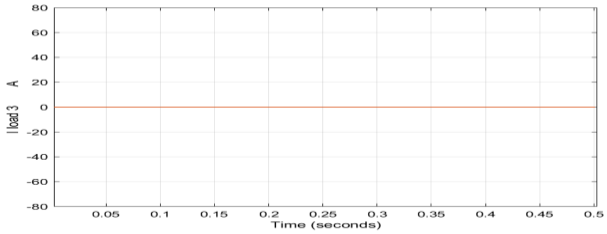

(a) Primary control

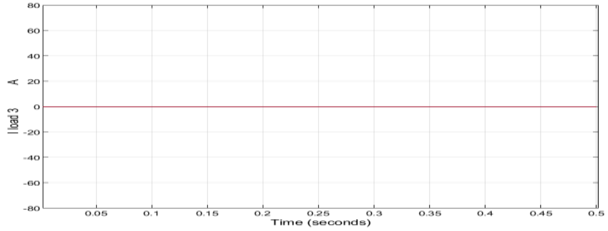

(b) Proposed control

Fig. 27 Iload 3 output in case (2)

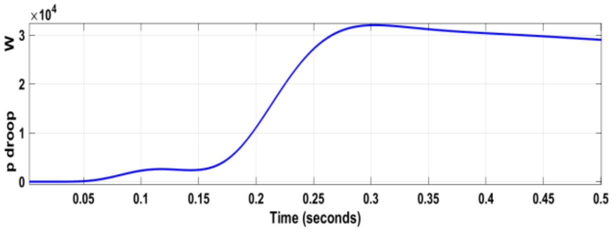

(a) Primary controller

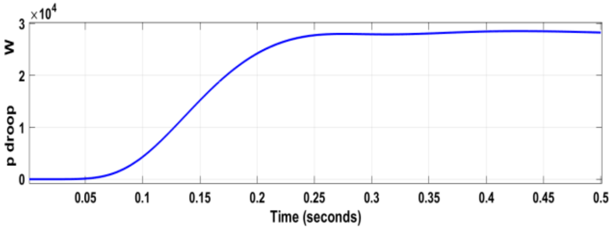

(b) Proposed control

Fig. 28 Droop active power in case (2)

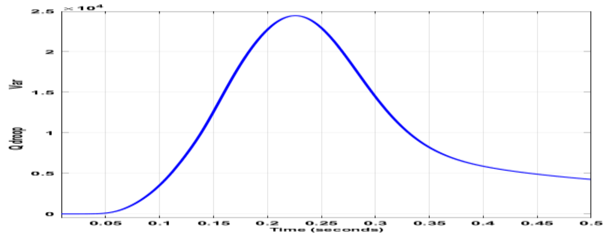

(a) Primary control

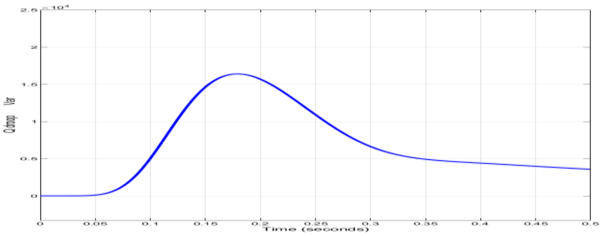

(b) Proposed control

Fig. 29 Droop reactive power in case (2)

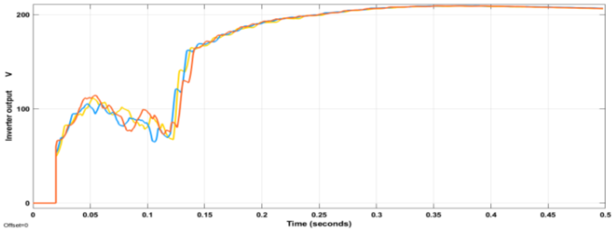

(a) Primary control

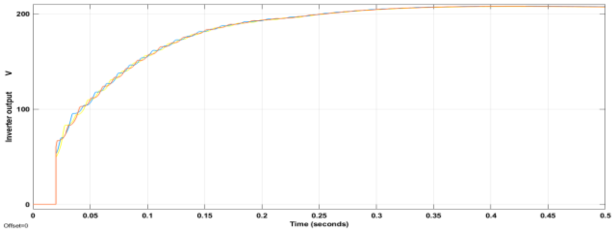

(b) Proposed control

Fig. 30 Inverter outputs in case (2)

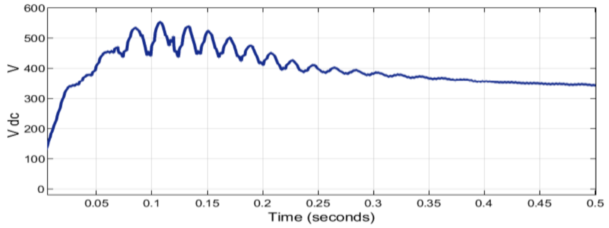

(a) Primary control

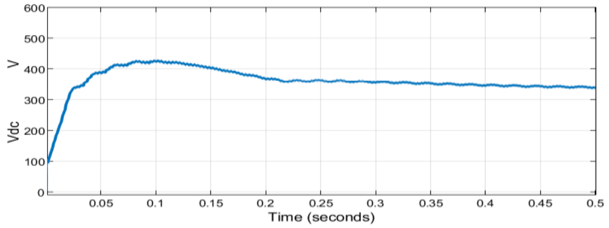

(b) Proposed control

Fig. 31 Vdc outputs in case (2)

9.3. Case (3) Increasing the SMG Load Values

This scenario investigates the hybrid smart microgrid under increased load conditions. The system response is evaluated in terms of voltage, frequency, active and reactive power levels of the connected loads. The application of the adaptive controller effectively suppresses oscillations in the smart microgrid voltage–frequency waveforms, leading to improved regulation of frequency, voltage, active, and reactive power. Moreover, the proposed control strategy ensures balanced power sharing among the distributed generators during steady-state operation, as demonstrated in Figures 32–44. Figure 32 compares the system frequency response obtained using the conventional controller and the proposed adaptive droop controller. Under primary droop control, the frequency exhibits pronounced oscillations ranging from 26.6 to 51.6 Hz. In contrast, the adaptive controller maintains the frequency close to its nominal value, stabilizing it at approximately 50.09 Hz.

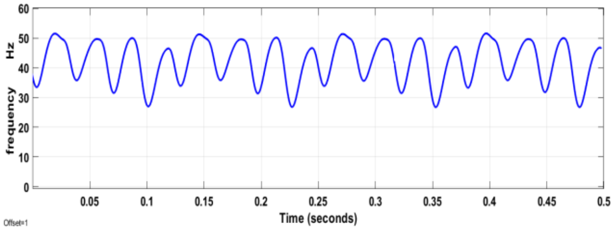

(a) Primary control

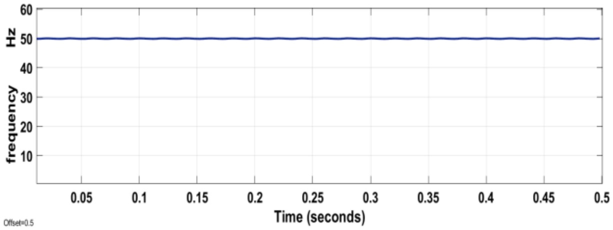

(b) Proposed control
Fig. 32 Frequency value in case (3)

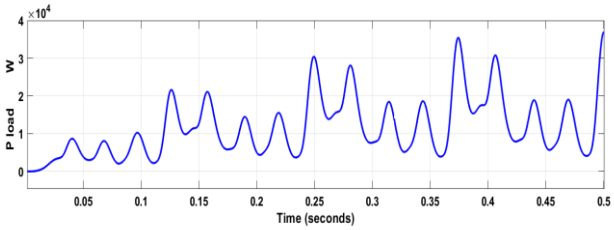

(a) Primary control

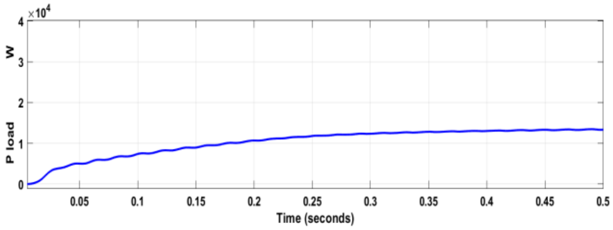

(b) Proposed control
Fig. 33 Load active power in case (3)

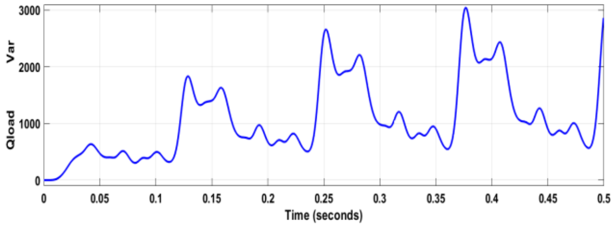

(a) Primary control

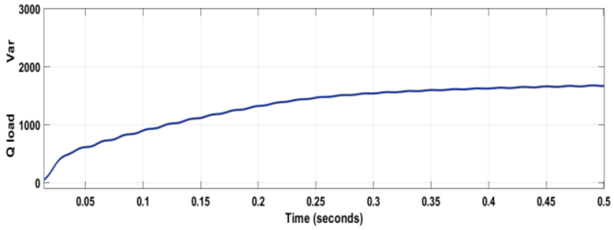

(b) Proposed control
Fig. 34 Load reactive power in case (3)

Figures 33 and 34 present a comparison of Pload and Qload responses of the load under both control strategies over the same time interval. As shown in Figure 33, Pload fluctuates significantly between 2,354 W and 37,878 W when regulated by the primary controller. By comparison, the proposed adaptive controller enables a smooth transition to a steady-state value of approximately 13,750 W. Similarly, Figure 34 illustrates that Qload oscillates between 319 and 3,050 Var under primary droop control, whereas the proposed controller regulates it to a stable steady-state value of about 1,710 Var. Overall, the results confirm that the proposed adaptive control strategy effectively suppresses oscillations and maintains system variables close to their nominal values under increased load conditions. Figures 35-40 illustrate Vload1, Vload2, Vload3, and Iload1, Iload2, and Iload3 waveforms for the three loads under two control approaches. In Figure 35, Vload1 oscillates between 65 V and 205 V when using the primary controller. With the proposed controller, Vload1 is stabilizing at a steady-state value of 153.5 V. Figure 36 shows that Iload1 oscillates between 55 and 220 A when controlled by the primary controller. In contrast, under the proposed controller, Iload1 holds smoothly to a steady-state value of 148 A.

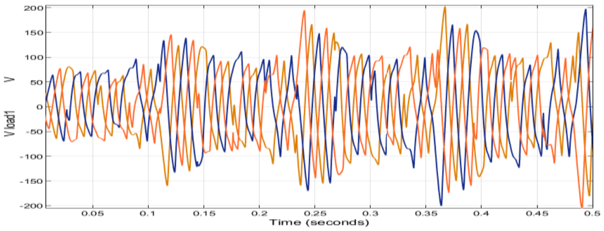

(a) Primary controller

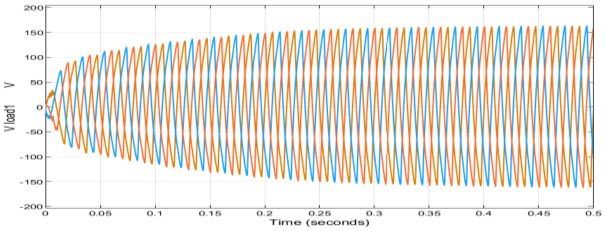

(b) Proposed controller
Fig. 35 Vload1 wave in case (3)

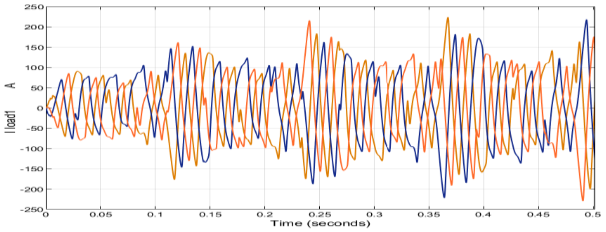

(a) Primary controller

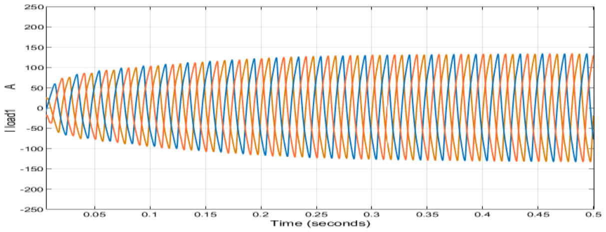

(b) Proposed control
Fig. 36 Iload 1 waves in case (3)

In Figure 37, Vload2 fluctuates between 64.5 V and 24.6 V under the primary controller. The proposed controller maintains Vload2 at a steady-state value of 152.8V. Figure 38 shows that Iload2 oscillates between 25 A and 81.6 A with the primary controller. Under the proposed controller, Iload2 has a steady-state value of 52 A. In Figure 39, Vload3 varies between 61 V and 203 V with the primary controller. The proposed controller achieves a steadier performance, maintaining Vload3 at 151V. Finally, Figure 40, illustrates that the current of load 3 (Iload3) fluctuates between 20 and 63 A when controlled by the conventional primary droop strategy. In contrast, the proposed adaptive controller regulates Iload3 to a steady-state value of approximately 35 A. Overall, under the proposed control scheme, the voltage and current waveforms exhibit near-sinusoidal characteristics with reduced oscillations and greater steadiness compared to the primary control case.

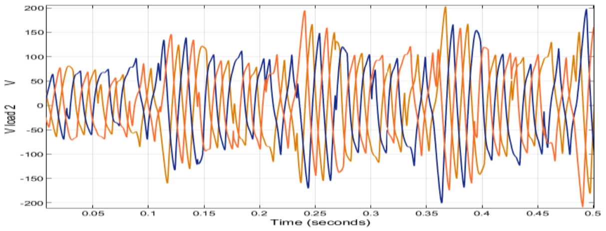

(a) Primary control

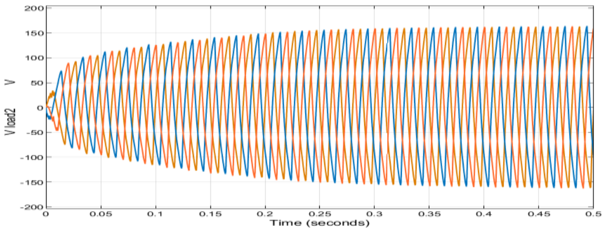

(b) Proposed control
Fig. 37 Vload 2 waves in case (3)

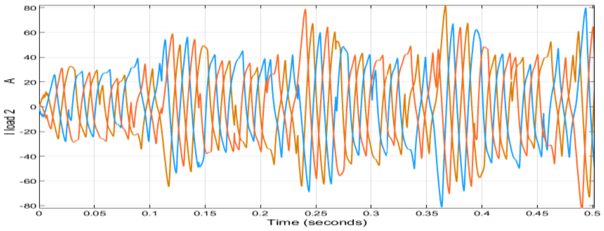

(a) Primary control

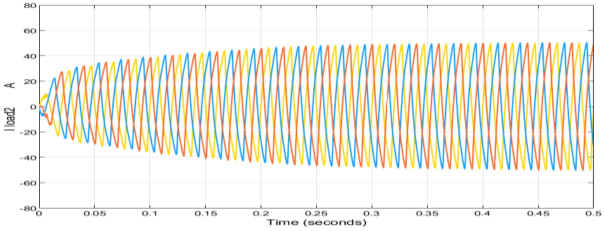

(b) Proposed control
Fig. 38 Iload 2 wave in case (3)

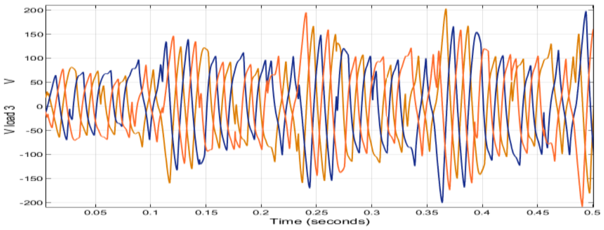

(a) Primary control

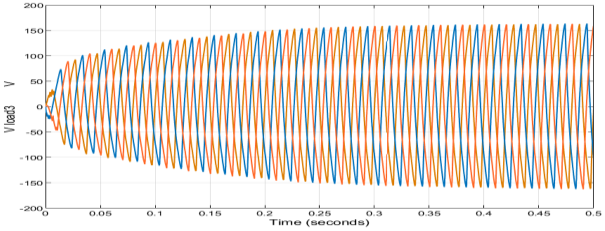

(b) Proposed control
Fig. 39 Vload 3 waves in case (3)

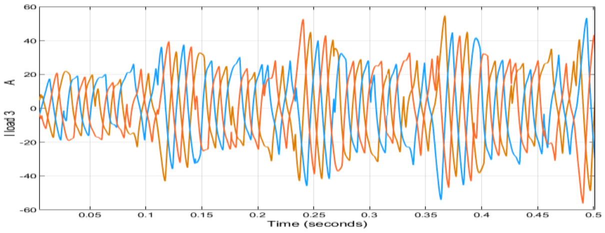

(a) Primary control

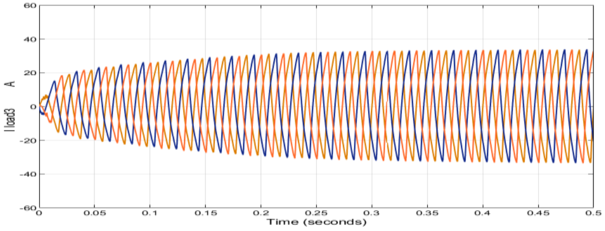

(b) Proposed control
Fig. 40 Iload 3 wave in case (3)

Figures 41-42, compare the performance of the two controllers in regulating Pdroop and Qdroop under two scenarios. In Figure 41, Pdroop exhibits oscillatory behavior ranging from 4,365 to 17,217 W under the primary controller. In contrast, with the proposed adaptive controller, Pdroop is adjusted to a steady value of 27,770 W. Figure 42 shows that Qdroop oscillates between 8,582 and 52,310 Var when using the primary controller. Under the proposed controller, Qdroop is adjusted to a steady value of 66044 Var.

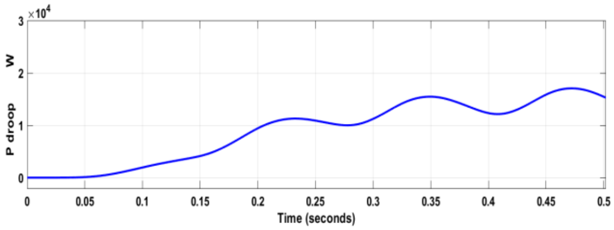

(a) Primary control

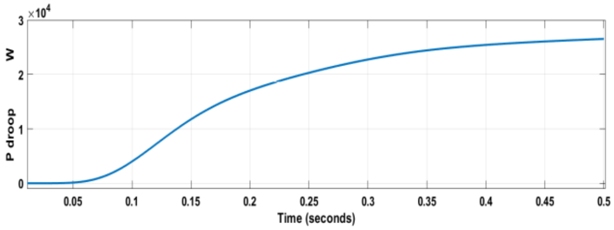

(b) Proposed control

Fig. 41 Droop active power output in case (3)

Figures 43-44 present the comparison of the inverter voltage waveform and Vdc under both control strategies. Figure 43, the inverter output oscillates between 35 and 129V with the primary controller. With the proposed controller, the inverter output maintains a steady-state value of 122 V. As shown in Figure 44, the DC-bus voltage (Vdc) varies between 450 and 665 V when regulated by the primary controller.

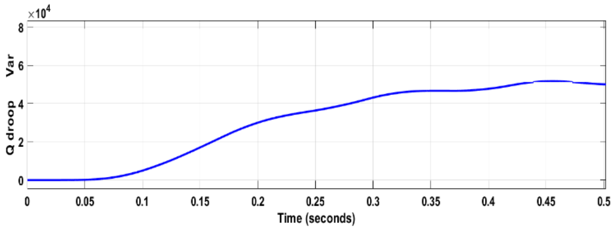

(a) Primary control

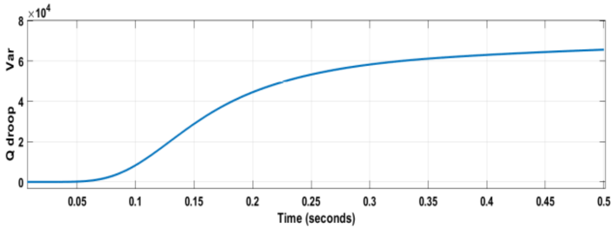

(b) Proposed control

Fig. 42 Droop reactive power output in case (3)

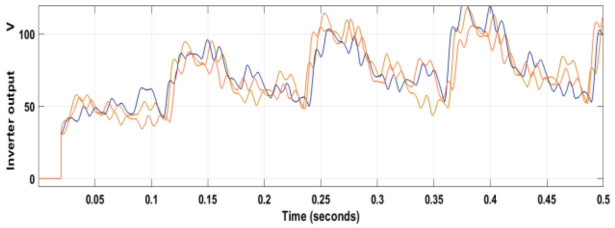

(a) Primary control

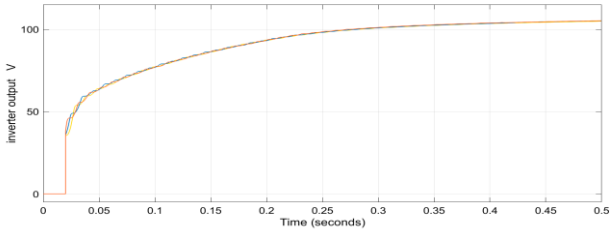

(b) Proposed control

Fig. 43 Inverter output in case (3)

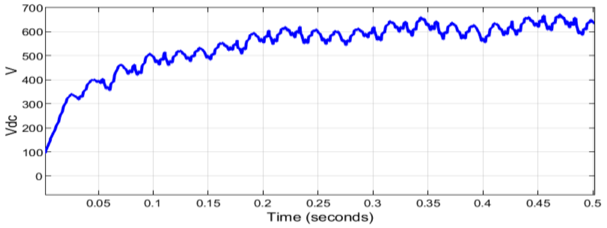

(a) Primary control

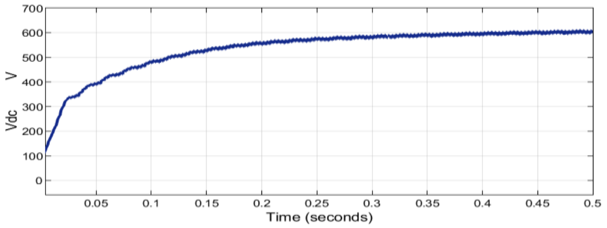

(b) Proposed control

Fig. 44 Vdc output in case (3)

In contrast, the proposed controller stabilizes Vdc at a steady-state value of approximately 621 V. These results indicate that, under the proposed control (case b), both inverter output and DC-bus voltage waveforms exhibit improved stability and reduced oscillations compared to the primary control case (case a).

10. Conclusion

This paper introduces an adaptive droop control strategy for hybrid smart microgrids aimed at enhancing the performance of the primary control layer, including droop, voltage, and current controllers. The proposed approach improves power quality by effectively regulating system frequency and voltage while preserving accurate active and reactive power sharing between interconnected smart microgrids. Owing to its simple implementation, the controller efficiently suppresses frequency and voltage deviations caused by load sharing among inverters and enhances overall power distribution in hybrid smart microgrid systems.

Simulation results obtained under three operating scenarios-steady-state operation, load disconnection, and increased load demand-demonstrate that the proposed adaptive droop controller significantly improves system stability margins and enables faster and more reliable power sharing. The results further confirm the controller's effectiveness in reducing voltage and frequency fluctuations across varying operating conditions. Overall, the proposed control strategy provides a robust and efficient solution to achieve power sharing and maintain system stability in inverter-based hybrid smart microgrid architectures. The future research directions are studying the performance of the adaptive droop control strategy in H-AC/DC- SMG under transient loading conditions and during system disturbances.

Author Contributions

All the authors have accepted responsibility for the entire content of this submitted manuscript and an approved submission.

Acknowledgments

The authors are grateful to the faculty of engineering, Mansoura University, El-Mansoura, Egypt, for providing the necessary facilities to carry out this work.

References

[1] Can Ding et al., "Research on Adaptive Bidirectional Droop Control Strategy for Hybrid AC-DC Microgrid in Islanding Mode," *Applied Sciences*, vol. 15, no. 15, pp. 1-21, 2025. [CrossRef] [Google Scholar] [Publisher Link]

[2] Rekha P. Nair, and Kanakasabapathy Ponnusamy, "Modeling and Simulation of Autonomous DC Microgrid with Variable Droop Controller," *Applied Sciences*, vol. 15, no. 9, pp. 1-13, 2025. [CrossRef] [Google Scholar] [Publisher Link]

[3] Atul S. Dahane, and Rajesh B. Sharma, "Hybrid AC-DC Microgrid Coordinated Control Strategies: A systematic Review and Future Prospect," *Renewable Energy Focus*, vol. 49, 2024. [CrossRef] [Google Scholar] [Publisher Link]

[4] Chang Yang et al., "A Communication-Saving Distributed Secondary Control of Hybrid AC/DC Microgrids and its Small-Signal Analysis," *Electric Power Systems Research*, vol. 229, 2024. [CrossRef] [Google Scholar] [Publisher Link]

[5] Galina Mirzaeva, and Dmitry Miller, "DC and AC Microgrids for Standalone Applications," *IEEE Transactions on Industry Applications*, vol. 59, no. 6, pp. 7908-7918, 2023. [CrossRef] [Google Scholar] [Publisher Link]

[6] Sina Ashrafi et al., "Control Strategy of Frequency and DC Voltage for Interfacing Converter of Hybrid AC/DC Microgrid based on Improved Virtual Synchronous Generator," *IET Renewable Power Generation*, vol. 19, no. 1, pp. 1-15, 2025. [CrossRef] [Google Scholar] [Publisher Link]

[7] Hyeong-Jun Yoo, Thai-Thanh Nguyen, and Hak-Man Kim, "Consensus-based Distributed Coordination Control of Hybrid AC/DC Microgrids," *IEEE Transactions on Sustainable Energy*, vol. 11, no. 2, pp. 629-639, 2019. [CrossRef] [Google Scholar] [Publisher Link]

[8] Ali Mahmoudian et al., "Adaptive Power-Sharing Strategy in Hybrid AC/DC Microgrid for Enhancing Voltage and Frequency Regulation," *International Journal of Electrical Power & Energy Systems*, vol. 156, pp. 1-15, 2024. [CrossRef] [Google Scholar] [Publisher Link]

[9] Farooq Alam et al., "Robust Hierarchical Control Design for the Power Sharing in Hybrid Shipboard Microgrids," *Inventions*, vol. 8, no. 1, pp. 1-26, 2022. [CrossRef] [Google Scholar] [Publisher Link]

[10] Mohammadreza Nabatirad, Reza Razzaghi, and Behrooz Bahrani, "Autonomous Power Balance in Hybrid AC/DC Microgrids," *International Journal of Electrical Power & Energy Systems*, vol. 146, 2023. [CrossRef] [Google Scholar] [Publisher Link]

[11] Jae-Won Chang et al., "A Novel Distributed Control Method for Interlinking Converters in an Islanded Hybrid AC/DC Microgrid," *IEEE Transactions on Smart Grid*, vol. 12, no. 5, pp. 3765-3779, 2021. [CrossRef] [Google Scholar] [Publisher Link]

[12] Lucas S. Araujo et al., "Heterogeneous Microgrids: Centralized Control Strategy with Distributed Grid-forming Converters," *International Journal of Electrical Power & Energy Systems*, vol. 158, pp. 1-15, 2024. [CrossRef] [Google Scholar] [Publisher Link]

[13] Jun Yang, Wenyue Luo, and Junhao Hou, "Distributed Optimal Control of AC/DC Hybrid Microgrid Groups with Interlinking Converters," *Journal of Electrical Engineering & Technology*, vol. 19, no. 7, pp. 3947-3965, 2024. [CrossRef] [Google Scholar] [Publisher Link]

[14] Rajind Chamika Samaraweera, and Nicoloy Gurusinghe, "Harmonic Compensation in Single-Phase Multilevel Grid-Forming Inverters for DC-coupled Microgrids," *Authorea Preprints*, *IEEE Open Journal of the Industrial Electronics Society*, vol. 20, no. 1, pp. 1-18, 2025. [CrossRef] [Google Scholar] [Publisher Link]

[15] Farahnaz Ahmadi, Yazdan Batmani, and Hassan Bevrani, "Model Reference Adaptive Controller for Simultaneous Voltage and Frequency Restoration of Autonomous AC Microgrids," *Journal of Modern Power Systems and Clean Energy*, vol. 12, no. 4, pp. 1194-1202, 2024. [CrossRef] [Google Scholar] [Publisher Link]

[16] Jae-Won Chang, Jae-Young Park, and Pyeong-Ik Hwang, "Decentralized Secondary Control of DGs for an Islanded Hybrid AC/DC Microgrid," *IEEE Access*, vol. 12, pp. 3597-3610, 2024. [CrossRef] [Google Scholar] [Publisher Link]

[17] Paulo T. de Godoy et al., "Unified Centralized/Decentralized Voltage and Frequency Control Structure for Microgrids," *Sustainable Energy, Grids and Networks*, vol. 38, 2024. [CrossRef] [Google Scholar] [Publisher Link]

[18] Makireddi Ramana et al., “Sector Wise Modified Droop Control to Improve Voltage Regulation and Current Sharing in Parallel Boost Converter Interfaced DC Microgrid,” *IEEE Journal of Emerging and Selected Topics in Power Electronics*, vol. 13, no. 3, pp. 2928-2943, 2024. [CrossRef] [Google Scholar] [Publisher Link]

[19] Nima Khosravi, “A Hybrid Control Approach to Improve Power Quality in Microgrid Systems,” *Artificial Intelligence Review*, vol. 58, no. 10, pp. 1-39, 2025. [CrossRef] [Google Scholar] [Publisher Link]

[20] Shumin Zong, Juerui Cao, and Can Wang, “Adaptive Normalized Droop control for Low-Voltage Hybrid Microgrid Interlinking Converter,” *Energy Reports*, vol. 9, pp. 1377-1388, 2023. [CrossRef] [Google Scholar] [Publisher Link]

[21] Mohammad S. Golsorkhi, and Mehdi Savaghebi, “A Decentralized Control Strategy Based on VI Droop for Enhancing Dynamics of Autonomous Hybrid AC/DC Microgrids,” *IEEE Transactions on Power Electronics*, vol. 36, no. 8, pp. 9430-9440, 2021. [CrossRef] [Google Scholar] [Publisher Link]

[22] Tanushree Rai, Anurag Tripathi, and Anurag Verma, “Voltage Stability at PCC in Islanded System using Droop Control Technique,” *2024 IEEE 11th Uttar Pradesh Section International Conference on Electrical, Electronics and Computer Engineering (UPCON)*, Lucknow, India, pp. 1-6, 2024. [CrossRef] [Google Scholar] [Publisher Link]

[23] Widi Aribowo, Heri Suryoatmojo, and Feby Agung Pamuji, “Improved Droop Control based on Modified Osprey Optimization Algorithm in DC Microgrid,” *Journal of Robotics and Control (JRC)*, vol. 5, no. 3, pp. 804-820, 2024. [Google Scholar] [Publisher Link]

[24] Ahmed Rashwan, “A Modified Adaptive Droop Control for Improved Load Sharing in Microgrids Considering DG Boundary Limits,” *International Journal of Applied Energy Systems*, vol. 6, no. 1, pp. 1-11, 2024. [Google Scholar]

[25] Nourhan M. Dawoud, Tamer F. Megahed, and Sahar S. Kaddah, “Enhancing the Performance of Multi-Microgrid with High Penetration of Renewable Energy using Modified Droop Control,” *Electric Power Systems Research*, vol. 201, 2021. [CrossRef] [Google Scholar] [Publisher Link]

[26] Rabih A. Jabr, “Economic Operation of Droop-Controlled AC Microgrids,” *IEEE Transactions on Power Systems*, vol. 37, no. 4, pp. 3119-3128, 2021. [CrossRef] [Google Scholar] [Publisher Link]

[27] Carlos Gómez-Aleixandre et al., “Adaptive Droop Controller for a Hybrid 375 Vdc/48 Vdc/400 Vac AC/DC Microgrid,” *IEEE Transactions on Industry Applications*, vol. 58, no. 4, pp. 5104-5116, 2022. [CrossRef] [Google Scholar] [Publisher Link]

[28] Buddhadeva Sahoo, Subhransu Ranjan Samantaray, and Mohammed M. Alhaider, “Advanced Control Scheme for Harmonic Mitigation and Performance Improvement in DC-AC Microgrid with Parallel Voltage Source Inverter,” *Scientific Reports*, vol. 15, no. 1, pp. 1-19, 2025. [CrossRef] [Google Scholar] [Publisher Link]

[29] Kandukuri Surendra, Biswarup Das, and Vinay Pant, “Interval Load Flow Models for Islanded AC and Hybrid AC/DC Microgrids with Load Uncertainties,” *IEEE Transactions on Industry Applications*, vol. 61, no. 5, pp. 7880-7891, 2025. [CrossRef] [Google Scholar] [Publisher Link]

[30] Sumit Kumar Jha, Deepak Kumar, and M. Lehtonen, “Modified VI Droop based Adaptive Vector Control Scheme for Demand Side Management in a Stand-Alone Microgrid,” *International Journal of Electrical Power & Energy Systems*, vol. 130, 2021. [CrossRef] [Google Scholar] [Publisher Link]

[31] Ahmed Tazy, Mohamed Mahmoud Samy, and Mohamed Ali Ghalib, “Enhancement and Control of Reactive Power Sharing Utilizing Circulating Current in AC Microgrids,” *2022 23rd International Middle East Power Systems Conference (MEPCON)*, Cairo, Egypt, pp. 1-5, 2022. [CrossRef] [Google Scholar] [Publisher Link]

[32] Chiebuka Eyisi, and Qifeng Li, “Analysis and Optimization of Boost Converter Parameters in Internal Model-based Control of Voltage Source Converter-based AC Microgrids,” *CSEE Journal of Power and Energy Systems*, vol. 10, no. 5, pp. 2038-2054, 2023. [CrossRef] [Google Scholar] [Publisher Link]

[33] Mobin Naderi et al., “Comprehensive Small-Signal Modeling and Prony Analysis-Based Validation of Synchronous Interconnected Microgrids,” *Energy Reports*, vol. 7, pp. 6677-6689, 2021. [CrossRef] [Google Scholar] [Publisher Link]

[34] Mehdi Baharizadeh, Mohammad Sadegh Golsorkhi Esfahani, and Nader Kazemi, “Modified Virtual Frequency-Voltage Frame Control Scheme with Zero Sharing Error for Islanded AC Microgrids,” *IET Generation, Transmission & Distribution*, vol. 17, no. 11, pp. 2576-2586, 2023. [CrossRef] [Google Scholar] [Publisher Link]

[35] Y. Saeidinia et al., “Autonomous Control of DC Microgrid based on a hybrid Droop Control Scheme for Total Generation Cost and Transmission Power Loss Reduction,” *Electrical Engineering*, vol. 105, no. 1, pp. 267-283, 2023. [CrossRef] [Google Scholar] [Publisher Link]

[36] Md Abu Taher et al., “Recurrent Neural Network-based Sensor Data Attacks Identification in Distributed Renewable Energy-Based DC Microgrid,” *2024 IEEE Texas Power and Energy Conference (TPEC)*, College Station, TX, USA, pp. 1-6, 2024. [CrossRef] [Google Scholar] [Publisher Link]

[37] Amir Afshari et al., “Distributed Fault-tolerant Voltage/ Frequency Synchronization in Autonomous AC Microgrids,” *IEEE Transactions on Power Systems*, vol. 35, no. 5, pp. 3775-3789, 2020. [CrossRef] [Google Scholar] [Publisher Link]

[38] B. Chiranjeev Rao, and Shimpy Ralhan, "Microgrid System with Event Triggered Distributed Secondary Control," *2024 Fourth International Conference on Advances in Electrical, Computing, Communication and Sustainable Technologies (ICAECT)*, Bhilai, India, pp. 1-7, 2024. [CrossRef] [Google Scholar] [Publisher Link]

[39] Fatemeh Zare-Mirakabad, Mohammad-Hosein Kazemi, and Aref Doroudi, "Distributed Robust Control of Frequency and Active Power-Sharing Ratio Regulation in Islanded AC Microgrids," *Electrical Engineering*, vol. 106, no. 5, pp. 5909-5918, 2024. [CrossRef] [Google Scholar] [Publisher Link]

[40] Hao Liu et al., "Droop Control Strategy Without Interconnection Lines for Input-Parallel Output-Series Grid-Connected Inverter System," *IEEE Transactions on Industrial Electronics*, vol. 71, no. 11, pp. 15224-15228, 2024. [CrossRef] [Google Scholar] [Publisher Link]

[41] Laura Ward et al., "Analysis of Grid-Forming Inverter Controls for Grid-Connected and Islanded Microgrid Integration," *Sustainability*, vol. 16, no. 5, pp. 1-22, 2024. [CrossRef] [Google Scholar] [Publisher Link]

[42] M.J. Babaei et al., "A Distributed Finite Time based Secondary Average Controller for Voltage/Frequency Regulation and Active/Reactive Power Sharing of AC Microgrids," *International Journal of Engineering Transactions A: Basics*, vol. 38, no. 1, pp. 1-11, 2025. [CrossRef] [Google Scholar] [Publisher Link]

[43] Junyan Hu, and Parijat Bhowmick, "A Consensus-based Robust Secondary Voltage and Frequency Control Scheme for Islanded Microgrids," *International Journal of Electrical Power & Energy Systems*, vol. 116, pp. 1-14, 2020. [CrossRef] [Google Scholar] [Publisher Link]

[44] Sarra Adiche et al., "Advanced Control Strategy for AC Microgrids: A hybrid ANN-based Adaptive PI Controller with Droop Control and Virtual Impedance Technique," *Scientific Reports*, vol. 14, no. 1, pp. 1-44, 2024. [CrossRef] [Google Scholar] [Publisher Link]

[45] Ahmed Rashwan et al., "Modified Droop Control for Microgrid Power-Sharing Stability Improvement," *Sustainability*, vol. 15, no. 14, pp. 1-19, 2023. [CrossRef] [Google Scholar] [Publisher Link]